PHYSICAL REVIEW D **91,** 115019 (2015)

Investigation of dark matter in minimal 3-3-1 models

P. V. Dong[*]
Institute of Physics, Vietnam Academy of Science and Technology, 10 Dao Tan, Ba Dinh, Hanoi, Vietnam

C. S. Kim[†] and N. T. Thuy[‡]
Department of Physics and IPAP, Yonsei University, Seoul 120-479, Korea

D. V. Soa[§]
Department of Physics, Hanoi Metropolitan University, 98 Duong Quang Ham, Cau Giay, Hanoi, Vietnam
(Received 25 January 2015; published 24 June 2015)

We show that the 3-3-1 model with minimal lepton content can work as a two-Higgs-triplet 3-3-1 model while leaving the other scalars as inert particles responsible for dark matter. We study two cases of dark matter, corresponding to the doublet and singlet scalar candidates, and we determine the parameter spaces in the WMAP-allowed region of relic density. Indirect and direct searches for dark matter in both cases are investigated by using micrOMEGAs.

DOI: 10.1103/PhysRevD.91.115019 PACS numbers: 12.60.-i, 95.35.+d

I. INTRODUCTION

Cosmological observations [1] suggest that there must exist cold dark matter that contains approximately 27% of all energy density of the Universe. Dark matter is a mysterious and interesting subject in particle physics as well as in astrophysics. In the context of particle physics, the most popular dark-matter candidates include the lightest supersymmetric particle, the lightest KK particle, the lightest T-odd particle, the axion, some form of sterile neutrinos, inert scalars, and others [2].

The Standard Model is very successful in describing experimentally observed phenomena, but it leaves some unsolved problems, such as neutrino masses and mixing, matter-antimatter asymmetry, dark matter, dark energy, etc., which leads us to go beyond the Standard Model. One simple way to go beyond the Standard Model is to extend the gauge group $SU(2)_L \otimes U(1)_Y$ to $SU(3)_L \otimes U(1)_X$ [3,4]. The class of $SU(3)_C \otimes SU(3)_L \otimes U(1)_X$ (3-3-1) models has many interesting characteristics; for example, these models can explain the number of fermion generations, the uncharacteristically heavy top quark [5], the electric charge quantization [6], the light neutrino masses [7], and dark matter [8].

There are two main versions of the 3-3-1 model, depending on which type of particle is located at the bottom of the lepton triplets. The minimal 3-3-1 model [3] uses ordinary charged leptons e_R, while the version with right-handed neutrinos includes ν_R [4]. There is no dark-matter candidate in the original minimal 3-3-1 model, nor in the original 3-3-1 model with right-handed neutrinos, since the new particles in these models either are electrically charged or rapidly decay. A natural approach [9] is that the stability of dark matter is based on W parity (similar to R parity in supersymmetry) through considering the baryon minus lepton numbers as a local gauge symmetry. However, this mechanism works only with the 3-3-1 model with neutral fermions (N_R) that possess $L(N_R) = 0$ and $B(N_R) = 0$. Therefore, the issue of dark matter for the original 3-3-1 models remains unresolved.

If the $B - L$ charge [even for similar charges that do not commute with $SU(3)_L$] is conserved, the 3-3-1 models are not self-consistent, because the $B - L$ and 3-3-1 symmetries are algebraically nonclosed [9,10]. Hence, the 3-3-1 models are manifest only if they contain interactions that explicitly violate $B - L$ (this perspective views $B - L$ as an approximate symmetry). Because the normal Lagrangians of the 3-3-1 models—including the gauge interactions, minimal Yukawa Lagrangian, and minimal scalar potential —conserve $B - L$, the unwanted (abnormal) interactions that violate $B - L$ must be presented. Such an interaction provides the nonzero small masses for the neutrinos [11]. In this work, we argue that the existence of inert fields not only can make the 3-3-1 model viable, but also can provide realistic candidates for dark matter. In more detail, one might introduce a Z_2 symmetry so that one scalar triplet of the theory is odd, while all other fields are even under the Z_2 symmetry. Odd particles act as inert fields [12]; therefore, the lightest and neutral inert particle is stable and can be dark matter [10,11]. Inert fields communicate with normal fields via an interaction that violates $B - L$, and this interaction subsequently separates the masses of the inert fields that make the dark-matter candidate viable under the direct searches.

[*]pvdong@iop.vast.ac.vn
[†]Corresponding author.
cskim@yonsei.ac.kr
[‡]ntthuy@iop.vast.ac.vn
[§]dvsoa@assoc.iop.vast.ac.vn

 © 2015 American Physical Society

The minimal 3-3-1 model originally works with three scalar triplets $\rho = (\rho_1^+, \rho_2^0, \rho_3^{++})$, $\eta = (\eta_1^0, \eta_2^-, \eta_3^+)$, and $\chi = (\chi_1^-, \chi_2^{--}, \chi_3^0)$, and either with or without one scalar sextet $S = (S_{11}^0, S_{12}^-, S_{13}^+, S_{22}^{--}, S_{23}^0, S_{33}^{++})$. In order to enrich the inert scalar sector responsible for dark matter, one can consider the "reduced 3-3-1 model" [13] by excluding η and S, or the "simple 3-3-1 model" [11] by excluding ρ and S. Unfortunately, the reduced 3-3-1 model gives large flavor-changing neutral currents as well as a large ρ parameter because the new physics scale is limited by a low Landau pole of around 5 TeV. The approach with the simple 3-3-1 model seems to be more realistic, except for the discrepancy between the flavor-changing neutral current and ρ-parameter constraints (this, however, has not really ruled out the model) [14]. Additional inert scalars can be a triplet ρ or sextets (S, σ), or a replication of η or χ. Among these proposals, the simple 3-3-1 model with inert scalar sextet σ [that has $X = 1$, where X is the charge of $U(1)_X$] or with the replication of η or χ can provide realistic dark-matter candidates. Dark-matter candidates for the model with inert σ have already been studied in [11]. In this work, we focus on dark matter in the models with η and χ replications. We remind the reader that dark-matter candidates of the model with ρ and the model with S are ruled out by direct search constraints. Here, in these cases the candidates are degenerate in masses and the interactions of inert and normal sectors conserve $B - L$ [11].

As a result of $SU(3)_L \otimes U(1)_X$ symmetry, the normal interactions generally produce relevant, new particles in pairs, similar to superparticles in supersymmetry (cf. [9]). Therefore, the 3-3-1 models have been thought to provide dark-matter candidates in a similar manner [8]. The problem, however, is how to suppress or evade the unwanted interactions and vacuums that cause the fast decay of dark matter. Fregolente and Tonasse [8] discussed a scalar sector of the minimal 3-3-1 model, but their candidate turned out to be the Goldstone boson of Z', which is unstable. Even the corresponding Higgs field interpreted therein would decay into ordinary particles via its coupling to the Standard Model Higgs bosons, exotic quarks, and gauge bosons. Long and Lan and Filippi *et al.* [8] discussed the scalar sector of the 3-3-1 model with right-handed neutrinos; the candidate was the real or imaginary part of a neutral scalar bilepton. Since the dark-matter stability mechanism was not given, there is no reason why the bilepton cannot develop a vacuum expectation value (VEV), and the lepton-number-violating (renormalizable) interactions in the Yukawa Lagrangian and scalar potential will turn on. Thus, the real part will decay into ordinary particles via the coupling to the Standard Model Higgs bosons, while the real and imaginary parts decay into light quarks due to ordinary and exotic quark mixings. To keep the bilepton stable, Pires and Rodrigues da Silva [8] imposed the lepton-number symmetry, which subsequently suppressed all the unwanted interactions and vacuums. However, the problem was in generating the neutrino masses; this finally breaks or violates the symmetry (contradictory to the postulate), and this destabilizes the candidate (e.g., the five-dimensional interactions for neutrino masses mentioned therein will lead to dark-matter decays into light neutrinos). Mizukoshi *et al.* [8] introduced another lepton sector, along with a Z_2 symmetry or $U(1)_G$ for dark-matter stability. However, the Z_2 is broken by the Higgs vacuum, while $U(1)_G$ is broken by its nontrivial dynamics [9]. The correct stability mechanism should be a W parity as the residual gauge symmetry. However, this works only with a new lepton sector as well as the inclusion of $B - L$ as a gauge symmetry. To conclude, the identification of dark matter and its stability for typical 3-3-1 models remain unsolved, which have called for our attention. The advantage of inert fields is that the dark-matter and neutrino masses can be simultaneously understood.

Our paper is organized as follows: In Sec. II, we briefly describe minimal 3-3-1 models that behave as the simple 3-3-1 model, and versions with η and χ replications. We also calculate the interactions of inert particles with the normal matter sector. In Sec. III, we present the dark-matter relic density and experimental searches for those two models. Finally, we summarize our work in Sec. IV.

II. BRIEF DESCRIPTION OF MINIMAL 3-3-1 MODELS

A. The simple 3-3-1 model

The fermions of the simple 3-3-1 model are arranged as [11]

$$\psi_{aL} \equiv \begin{pmatrix} \nu_{aL} \\ e_{aL} \\ (e_{aR})^c \end{pmatrix} \sim (1, 3, 0),$$
$$Q_{\alpha L} \equiv \begin{pmatrix} d_{\alpha L} \\ -u_{\alpha L} \\ J_{\alpha L} \end{pmatrix} \sim (3, 3^*, -1/3),$$
$$Q_{3L} \equiv \begin{pmatrix} u_{3L} \\ d_{3L} \\ J_{3L} \end{pmatrix} \sim (3, 3, 2/3), \tag{1}$$

$$u_{aR} \sim (3, 1, 2/3), \qquad d_{aR} \sim (3, 1, -1/3),$$
$$J_{\alpha R} \sim (3, 1, -4/3), \qquad J_{3R} \sim (3, 1, 5/3), \tag{2}$$

where $a = 1, 2, 3$ and $\alpha = 1, 2$ are family indices. The quantum numbers in parentheses are defined upon the gauge symmetries $SU(3)_C, SU(3)_L, U(1)_X$, respectively.

The electric charge operator has the form $Q = T_3 - \sqrt{3}T_8 + X$, where $T_i (i = 1, 2 \ldots, 8)$ and X are the charges of $SU(3)_L$ and $U(1)_X$, respectively. The exotic

quarks have electric charges different from the usual ones, $Q(J_\alpha) = -4/3$ and $Q(J_3) = 5/3$.

The model works well with two scalar triplets [11] as

$$\eta = \begin{pmatrix} \frac{1}{\sqrt{2}}(u + S_1 + iA_1) \\ \eta_2^- \\ \eta_3^+ \end{pmatrix} \sim (1,3,0),$$
$$\chi = \begin{pmatrix} \chi_1^- \\ \chi_2^{--} \\ \frac{1}{\sqrt{2}}(\omega + S_3 + iA_3) \end{pmatrix} \sim (1,3,-1). \quad (3)$$

The scalar potential is given by

$$V_{\text{simple}} = \mu_1^2\eta^\dagger\eta + \mu_2^2\chi^\dagger\chi + \lambda_1(\eta^\dagger\eta)^2 + \lambda_2(\chi^\dagger\chi)^2 + \lambda_3(\eta^\dagger\eta)(\chi^\dagger\chi) + \lambda_4(\eta^\dagger\chi)(\chi^\dagger\eta), \quad (4)$$

where $\mu_{1,2}$ have dimension of mass, while $\lambda_{1,2,3,4}$ are dimensionless. These parameters satisfy

$$\mu_{1,2}^2 < 0, \qquad \lambda_{1,2,4} > 0,$$
$$-2\sqrt{\lambda_1\lambda_2} < \lambda_3 < \text{Min}\{2\lambda_1(\mu_2/\mu_1)^2, 2\lambda_2(\mu_1/\mu_2)^2\}. \quad (5)$$

The model contains four massive scalars, the respective masses of which were obtained in [11] as follows:

$$h \equiv c_\xi S_1 - s_\xi S_3, \qquad m_h^2 \simeq \frac{4\lambda_1\lambda_2 - \lambda_3^2}{2\lambda_2}u^2,$$
$$H \equiv s_\xi S_1 + c_\xi S_3, \qquad m_H^2 \simeq 2\lambda_2\omega^2,$$
$$H^\pm \equiv c_\theta\eta_3^\pm + s_\theta\chi_1^\pm, \qquad m_{H^\pm}^2 \simeq \frac{\lambda_4}{2}\omega^2, \quad (6)$$

with denotations $c_x = \cos(x), s_x = \sin(x), t_x = \tan(x)$ for any angle x. The mixing angles ξ, θ are defined as

$$t_\theta = \frac{u}{\omega}, \qquad t_{2\xi} \simeq \frac{\lambda_3 u}{\lambda_2\omega}. \quad (7)$$

There are eight Goldstone bosons $G_Z \equiv A_1$, $G_{Z'} \equiv A_3$, $G_W^\pm \equiv \eta_2^\pm$, $G_Y^{\pm\pm} \equiv \chi_2^{\pm\pm}$, and $G_X^\pm \equiv c_\theta\chi_1^\pm - s_\theta\eta_3^\pm$, which are eaten by eight massive gauge bosons Z, Z', $W^\pm$, $Y^{\pm\pm}$, and $X^\pm$ (see below), respectively. In the limit $u \ll \omega$, we have $\xi, \theta \to 0$, thus

$$h \simeq S_1, \qquad H \simeq S_3, \qquad H^\pm \simeq \eta_3^\pm, \qquad G_X^\pm \simeq \chi_1^\pm. \quad (8)$$

In the gauge sector, the gauge boson masses arise from the Lagrangian $\sum_{\Phi=\eta,\chi}(D_\mu\langle\Phi\rangle)^\dagger(D^\mu\langle\Phi\rangle)$, where the covariant derivative is defined as $D_\mu = \partial_\mu + ig_s t_i G_{i\mu} + igT_i A_{i\mu} + ig_X X B_\mu$, in which the gauge coupling constants g_s, g, and g_X and the gauge bosons $G_{i\mu}, A_{i\mu}$, and B_μ are associated with the 3-3-1 groups, respectively. The gauge bosons with their masses are respectively given by [11]

$$W^\pm \equiv \frac{A_1 \mp iA_2}{\sqrt{2}}, \qquad m_W^2 = \frac{g^2}{4}u^2,$$
$$X^\mp \equiv \frac{A_4 \mp iA_5}{\sqrt{2}}, \qquad m_X^2 = \frac{g^2}{4}(\omega^2 + u^2), \quad (9)$$

$$Y^{\mp\mp} \equiv \frac{A_6 \mp iA_7}{\sqrt{2}}, \qquad m_Y^2 = \frac{g^2}{4}\omega^2, \quad (10)$$

and for the neutral gauge bosons

$$A = s_W A_3 + c_W(-\sqrt{3}t_W A_8 + \sqrt{1 - 3t_W^2}B), \qquad m_A = 0,$$
$$Z_1 \simeq c_W A_3 - s_W(-\sqrt{3}t_W A_8 + \sqrt{1 - 3t_W^2}B), \qquad m_{Z_1}^2 \simeq \frac{g^2}{4c_W^2}u^2,$$
$$Z_2 \simeq \sqrt{1 - 3t_W^2}A_8 + \sqrt{3}t_W B, \qquad m_{Z_2}^2 \simeq \frac{g^2 c_W^2}{3(1 - 4s_W^2)}\omega^2, \quad (11)$$

where $s_W = e/g = t/\sqrt{1 + 4t^2}$, with $t = g_X/g$, is the sine of Weinberg angle [15]. The photon field A_μ is exactly massless. For the gauge bosons Z_1, Z_2 we have taken the limit $u \ll \omega$. The Z_1 is identified as the Standard Model Z. The VEV u is constrained by the mass of W, thus $u \simeq 246$ GeV.

The Yukawa Lagrangian is given by

$$\mathcal{L}_Y = h_{33}^J\bar{Q}_{3L}\chi J_{3R} + h_{\alpha\beta}^J\bar{Q}_{\alpha L}\chi^* J_{\beta R} + h_{3a}^u\bar{Q}_{3L}\eta u_{aR} + \frac{h_{\alpha a}^u}{\Lambda}\bar{Q}_{\alpha L}\eta\chi u_{aR} + h_{\alpha a}^d\bar{Q}_{\alpha L}\eta^* d_{aR} + \frac{h_{3a}^d}{\Lambda}\bar{Q}_{3L}\eta^*\chi^* d_{aR}$$
$$+ h_{ab}^e\bar{\psi}_{aL}^c\psi_{bL}\eta + \frac{h_{ab}'^e}{\Lambda^2}(\bar{\psi}_{aL}^c\eta\chi)(\psi_{bL}\chi^*) + \frac{s_{ab}^\nu}{\Lambda}(\bar{\psi}_{aL}^c\eta^*)(\psi_{bL}\eta^*) + \text{H.c.}, \quad (12)$$

where the Λ is a new scale with the mass dimension. All the couplings, denoted by h's, conserve $B - L$, except that s^ν violates L by two units. The s^ν coupling can generate small masses for the neutrinos [11].

Let us introduce a Z_2 symmetry where all fields of the simple 3-3-1 model are assigned as even under the Z_2. Below, we consider replication of the simple 3-3-1 model by adding an extra scalar triplet, i.e., either η' or χ' assigned as an odd field under the Z_2.

B. The simple 3-3-1 model with η replication

An extra scalar triplet that replicates η is defined as

$$\eta' = \begin{pmatrix} \frac{1}{\sqrt{2}}(H_1' + iA_1') \\ \eta_2'^{-} \\ \eta_3'^{+} \end{pmatrix} \sim (1,3,0). \tag{13}$$

We notice that η' and η have the same gauge quantum numbers. However, η' is assigned as an odd field under the Z_2, $\eta' \to -\eta'$, so $\langle \eta' \rangle = 0$.

The scalar potential includes the V_{simple} given in Eq. (4) and the terms contained η',

$$\begin{aligned} V_{\eta'} &= \mu_{\eta'}^2 \eta'^{\dagger}\eta' + x_1(\eta'^{\dagger}\eta')^2 + x_2(\eta^{\dagger}\eta)(\eta'^{\dagger}\eta') \\ &\quad + x_3(\chi^{\dagger}\chi)(\eta'^{\dagger}\eta') + x_4(\eta^{\dagger}\eta')(\eta'^{\dagger}\eta) + x_5(\chi^{\dagger}\eta')(\eta'^{\dagger}\chi) \\ &\quad + \frac{1}{2}[x_6(\eta'^{\dagger}\eta)^2 + \text{H.c.}]. \end{aligned} \tag{14}$$

Here, $\mu_{\eta'}$ has mass dimension, while $x_i (i = 1,2,3,\ldots,6)$ are dimensionless. All the x_6, u, and ω can be considered to be real.

The model requires [10]

$$\mu_{\eta'}^2 > 0, \qquad x_{1,3} > 0, \qquad x_2 + x_4 \pm x_6 > 0. \tag{15}$$

The gauge states H_1', A_1', $\eta_2'^{\pm} \equiv H_2'^{\pm}$, and $\eta_3'^{\pm} \equiv H_3'^{\pm}$ by themselves are physically inert particles with corresponding masses as follows:

$$\begin{aligned} m_{H_1'}^2 &= M_{\eta'}^2 + \frac{1}{2}(x_4 + x_6)u^2, \\ m_{A_1'}^2 &= M_{\eta'}^2 + \frac{1}{2}(x_4 - x_6)u^2, \\ m_{H_2'^{\pm}}^2 &= M_{\eta'}^2, \qquad m_{H_3'^{\pm}}^2 = M_{\eta'}^2 + \frac{1}{2}x_5\omega^2, \end{aligned} \tag{16}$$

where $M_{\eta'}^2 \equiv \mu_{\eta'}^2 + \frac{1}{2}x_2u^2 + \frac{1}{2}x_3\omega^2$. If H_1' (or A_1') is the lightest inert particle (LIP), it can be the dark-matter candidate.

All the interactions in Eq. (14) conserve $B - L$ except that of x_6, since in principle the η' fields can have arbitrary $B - L$ charges. This is analogous to the case of the 3-3-1 model with right-handed neutrinos [10]. The masses of H_1' and A_1' are separated by x_6. Otherwise, the conservation of $B - L$, i.e., $x_6 = 0$, rules out the candidates H_1' and A_1' because they possess a large scattering cross section off nuclei due to the t-channel exchange by the Z boson [16].

Let us calculate the interactions of inert particles with normal ones. Because of the Z_2 symmetry, inert scalars interact only with normal scalars and gauge bosons, not with fermions. Details of the interactions are given in Appendix A.

Under the Standard Model symmetry, the candidates H_1', A_1' transform as a $SU(2)_L$ doublet, analogous to the ones of the inert doublet model [12]. However, our candidates are distinguishable due to the following two points: (i) Since ω is the 3-3-1 breaking scale fixed at TeV range [11], the candidates that have masses $\sim\omega$ are naturally heavy. However, note also that their masses depend on the scalar couplings as well as the $\mu_{\eta'}$ parameter. (ii) Besides the interactions with the Standard Model particles, the candidates have new interactions with the new gauge and Higgs bosons. That is, in the large mass region the dark-matter observables can be governed by new physics of the 3-3-1 model.

C. The simple 3-3-1 model with χ replication

The χ replication takes the form

$$\chi' = \begin{pmatrix} \chi_1'^{-} \\ \chi_2'^{--} \\ \frac{1}{\sqrt{2}}(H_3' + iA_3') \end{pmatrix} \sim (1,3,-1). \tag{17}$$

The χ' is assigned as odd under the Z_2 symmetry that requires $\langle \chi' \rangle = 0$. The additional potential into Eq. (4) due to the χ' field is given as

$$\begin{aligned} V_{\chi'} &= \mu_{\chi}^2 \chi'^{\dagger}\chi' + y_1(\chi'^{\dagger}\chi')^2 + y_2(\eta^{\dagger}\eta)(\chi'^{\dagger}\chi') \\ &\quad + y_3(\chi^{\dagger}\chi)(\chi'^{\dagger}\chi') + y_4(\eta^{\dagger}\chi')(\chi'^{\dagger}\eta) + y_5(\chi^{\dagger}\chi')(\chi'^{\dagger}\chi) \\ &\quad + \frac{1}{2}[y_6(\chi'^{\dagger}\chi)^2 + \text{H.c.}]. \end{aligned} \tag{18}$$

To make sure the scalar potential is bounded from below and the Z_2 is conserved by the vacuum, we impose

$$\mu_{\chi'}^2 > 0, \qquad y_{1,2} > 0, \qquad y_3 + y_5 \pm y_6 > 0. \tag{19}$$

The physical inert scalars H_3', A_3', $\chi_1'^{\pm} \equiv H_1'^{\pm}$, and $\chi_2'^{\pm\pm} \equiv H_2'^{\pm}$ with the respective masses are obtained as

$$\begin{aligned} m_{H_3'}^2 &= M_{\chi'}^2 + \frac{1}{2}(y_5 + y_6)\omega^2, \\ m_{A_3'}^2 &= M_{\chi'}^2 + \frac{1}{2}(y_5 - y_6)\omega^2, \\ m_{H_2'^{\pm\pm}}^2 &= M_{\chi'}^2, \qquad m_{H_1'^{\pm}}^2 = M_{\chi'}^2 + \frac{1}{2}y_4u^2, \end{aligned} \tag{20}$$

where $M_{\chi'}^2 \equiv \mu_{\chi'}^2 + \frac{1}{2}y_2u^2 + \frac{1}{2}y_3\omega^2$. If H_3' (or A_3') is the LIP, it can be the dark-matter candidate.

The couplings $y_{1,2,3,4,5}$ conserve $B-L$, whereas y_6 violates this charge because χ' can have arbitrary $B-L$ charges. The masses of H_3' and A_3' are separated by y_6, similar to the previous case. If their masses are degenerate, i.e., $B-L$ is conserved, there is a scattering of H_3' and A_3' off nuclei due to the t-channel exchange by the Z' boson. This cross section is also large because the Z' mass is limited by the Landau pole, which is experimentally unacceptable (this matter is analogous to the case of the sextet presented in [11]).

Let us consider the interactions of inert Higgs with normal Higgs as well as the gauge bosons. We remind the reader that inert scalars do not interact with fermions because of the invariance under the Z_2 symmetry. Details of interactions are given in Appendix B.

The candidates H_3' and A_3' transform as singlets under the Standard Model symmetry, similar to the phantom of Silveira-Zee model [17]. However, their physics is distinguishable due to the interactions with the new gauge and Higgs bosons, in addition to the Standard Model Higgs portal. The dark-matter observables in their large mass range can be governed by the new physics; since the candidates have masses proportional to ω, they have natural masses in the TeV range. Please note that their masses depend on the scalar couplings as well as the $\mu_{\chi'}$ parameter.

III. DARK MATTER IN MINIMAL 3-3-1 MODELS

Let us recall that the simple 3-3-1 model with an inert ρ triplet and the model with inert scalar sextets were previously considered in [11]. In this work, we study dark matter in the simple 3-3-1 model with η replication (which we call the η' model) and the model with χ replication (called the χ' model) in detail.

In order to calculate the relic density as well as indirect and direct searches for dark matter, we use micrOMEGAs [18,19] after expanding the relevant interactions and implementing new model files in CalcHEP [20]. All possible annihilation and coannihilation channels are considered in the computation of relic density. The coannihilation may reduce the relic density significantly if the mass of inert particles exists within around 10%, or even 20%, of the LIP mass [21].

Dark-matter annihilation produces pairs of Standard Model particles (or new particles, in our model) that hadronize and decay into stable particles. Indirect search observes the signals of positrons, antiprotons, and gamma rays that are finally produced in dark-matter annihilation processes. MicrOMEGAs computes the photon, positron, and antiproton flux at a given energy E and the angle of the direction of observation (this can be the source for experiments such as PAMELA, Fermi, etc.).

In direct searches, one measures the recoil energy deposited by the scattering of LIPs with the nuclei. In this work, both the η' model and the χ' model provide Higgs dark matter that can only contribute to the spin-independent interactions with the nuclei. To derive the LIP-nucleus cross section, we use the method mentioned in [19]. All interactions of the LIP with quarks are input in the model files; CalcHEP then generates and calculates all diagrams for LIP-quark and -antiquark elastic scattering at zero momentum. The normalized cross section on a pointlike nucleus is obtained as

$$\sigma^{\rm SI}_{\rm LIP-N} = \frac{4\mu^2_{\rm LIP}}{\pi}(Z\lambda_p + (A-Z)\lambda_n)^2, \tag{21}$$

where $\mu_{\rm LIP}$ is the LIP-nucleus reduced mass, $\mu_{\rm LIP} = m_{\rm LIP}m_{\rm nuclei}/(m_{\rm LIP}+m_{\rm nuclei}) \simeq m_{\rm nuclei}$. λ_p and λ_n are the effective couplings of the LIP to protons and neutrons, respectively. The couplings $\lambda_{p,n}$ are connected to the coefficients f^N_q, which are linked to the pion-nucleon sigma term $\sigma_{\pi N}$ and the quantity σ_0 [19]. Recent analyses suggest that [22]

$$\sigma_{\pi N} = 55-73\ \text{MeV}, \qquad \sigma_0 = 35\pm 5\ \text{MeV}. \tag{22}$$

The direct rate does not change as much in the above ranges of $\sigma_{\pi N}$ and σ_0. The results of the relic density as well as of searches for dark matter in each model are presented in subsections below.

A. Dark matter in the simple 3-3-1 model with η replication

The inert particles in the simple 3-3-1 model with η replication are $H_1', A_1', H_2'^{\pm}$, and $H_3'^{\pm}$. With the condition $x_6 < \min\{0, -x_4, (\omega/u)^2 x_5 - x_4\}$, H_1' is the LIP, and can be a candidate for dark matter. See Appendix C for possible (co)annihilation channels of H_1'.

The η' model contains the following parameters: $\mu^2_{\eta'}, \omega, \lambda_{1,2,3,4}$, and $x_{1,2,3,4,5,6}$. Let us choose some fixed ones as

$$\lambda_2 = \lambda_3 = \lambda_4 = 0.1, \qquad x_1 = 0.01, \qquad x_2 = 0.03,$$
$$x_3 = 0.01, \qquad x_4 = 0.07, \qquad x_5 = 0.08, \qquad x_6 = -0.09. \tag{23}$$

The coupling λ_1 is constrained by the mass of the Standard Model Higgs, $m_h = 125$ GeV. The squared-mass splittings of inert fields are obviously defined, where the doublet components (H_1', A_1', H_2') are slightly separated due to the weak scale, but they are largely separated from the singlet H_3' by the ω scale.

From Eq. (16), the dark-matter mass depends on the two parameters $\mu_{\eta'}$ and ω. By our choice, the ω term of the dark-matter mass is $\sqrt{\frac{x_3}{2}}\omega \simeq 0.07\omega$, which is given at the weak scale for ω in a few TeV. Therefore, the dark-matter mass ranges from the weak scale to the TeV scale for $\mu_{\eta'}$ varying correspondingly on such a range. This selection

of the dark-matter mass region will scan all contributions of the Standard Model and 3-3-1 models to the dark-matter relic density [this is because (co)annihilation precesses open when the dark matter is heavier than its product].

The simple 3-3-1 model inherits two distinct regions of mass spectrum: (1), given at the weak scale (u) of the Standard Model particles such as t, h, Z, W, and so on; and (2), achieved at the TeV scale (ω) of new particles, including X, Y, Z', $J_{1,2,3}$, H^0, and $H^\pm$. Notice that for $\omega = 3-5$ TeV [11], X, Y, Z', H^0 (and assumed $J_{1,2,3}$) all have mass beyond 1 TeV. However, $H^\pm$ is slightly lighter, $m_{H^\pm} \simeq 0.67-1.12$ TeV. This is due to the particular choice of the scalar couplings. Of course, one can investigate the case where all the new scalars are heavy. Indeed, the conclusions given below remain unchanged.

Figure 1 shows the relic density as a function of dark-matter mass by varying $\mu_{\eta'}$ from 100 to 5000 GeV for $\omega = 3$ TeV (red), $\omega = 4$ TeV (green), and $\omega = 5$ TeV (blue). For each value of ω, there are three regions of dark-matter mass yielding right abundances ($\Omega h^2 \leq 0.1120 \pm 0.0056$ [23], where h is the reduced Hubble constant, which should not be confused with the Higgs field as given at outset).

(1) The first region: $m_{H_1'} < 600$ GeV. The relic density in this regime is governed by the Standard Model gauge and Higgs portals with only the Standard Model productions. Therefore, the relic density is independent of ω, the 3-3-1 breaking scale. All these contributions can be theoretically computed, which yields the effective, thermally averaged annihilation cross section times velocity as [24]

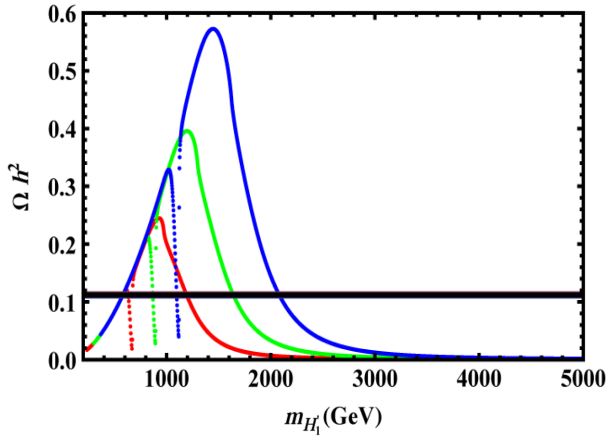

FIG. 1 (color online). Ωh^2 as a function of $m_{H_1'}$ for $\omega = 3$ TeV (red), $\omega = 4$ TeV (green), and $\omega = 5$ TeV (blue). The three curved lines are coincident at low-mass region and separated at the TeV scale for $\omega = 3$ TeV, $\omega = 4$ TeV, and $\omega = 5$ TeV, respectively, from left to right. The dotted lines are rare regions for $\omega = 3$ TeV (left), $\omega = 4$ TeV (middle), and $\omega = 5$ TeV (right). The horizontal line is the WMAP limit on the relic density.

$$\langle \sigma v \rangle \simeq \left(\frac{\alpha}{150\ \text{GeV}}\right)^2 \left[\left(\frac{600\ \text{GeV}}{m_{H_1'}}\right)^2 + \left(\frac{x \times 1.354\ \text{TeV}}{m_{H_1'}}\right)^2\right], \quad (24)$$

where $(\alpha/150\ \text{GeV})^2 \simeq 1$ pb, $x \equiv \sqrt{x_2^2 + x_4^2 + x_6^2}$, and the first and second terms in the brackets come from the gauge and Higgs portals, respectively. Because the Higgs couplings are small, $x \simeq 0.11$, the Higgs portal contributes negligibly. Hence, the relic density is governed by the gauge portal, which leads to $m_{H_1'} \simeq 600$ GeV in order to recover the correct abundance, $\Omega h^2 \simeq 0.1\ \text{pb}/\langle \sigma v \rangle \simeq 0.11$. This matches the result given by micrOMEGAs. From Fig. 1, we see that the three lines coincide at the region below 600 GeV for $\omega = 3, 4$, or 5 TeV, as predicted. This implies that we can have a dark-matter candidate with a mass of just or below 600 GeV, in agreement with the WMAP results on the relic density; this is independent with the new physics of the simple 3-3-1 model. The simple 3-3-1 model as well as the inert fields play the new role in the next two regions.

(2) The second region: H resonance. This regime for the dark-matter relic density is very narrow, as can be seen by the dotted lines in Fig. 1. It is due to an H resonance through the s-channel annihilation of the dark matter into Standard Model particles, including $H^\pm$ if kinematically allowed, by H exchange (note that H is a new Higgs of the simple 3-3-1 model). In other words, the relic density for this regime is set by the H resonance with the dark-matter mass around $m_{H_1'} = \frac{1}{2} m_H = \sqrt{\frac{\lambda_2}{2}}\omega$, which yields $m_{H_1'} \simeq 670$ GeV for $\omega = 3$ TeV, $m_{H_1'} \simeq 895$ GeV for $\omega = 4$ TeV, and $m_{H_1'} \simeq 1.118$ TeV for $\omega = 5$ TeV. The resonant points (dark-matter mass) as seen in the figure coincide with the given estimation. On the other hand, all the new particles of the simple 3-3-1 model are heavier than 1 TeV, except $H^\pm$ which has a mass of 670 GeV to 1.12 TeV for $\omega = 3-5$ TeV, as mentioned above. Therefore, only the $H^\pm$ channel can be additionally opened to give a small contribution to the relic density in this range (from 600 GeV to the point before the other new particles of the simple 3-3-1 model enter the product of dark-matter annihilation, a point which depends on the size of ω). Despite this contribution, the relic density radically increases and overpopulates out of the resonance regime, since the dark-matter mass increases.

(3) The third region: the 3-3-1 region. When the dark-matter mass reaches various masses of the new

particles of the simple 3-3-1 model, the corresponding annihilation channels open, and the dark-matter candidate can annihilate into the new gauge bosons, new Higgs bosons, and exotic quarks. Because of the numerous contributions, the relic density decreases to the correct abundance, with the values of dark-matter mass evaluated as follows: $m_{H_1'} \geq 1.15$ TeV for $\omega = 3$ TeV, $m_{H_1'} \geq 1.6$ TeV for $\omega = 4$ TeV, and $m_{H_1'} \geq 2.05$ TeV for $\omega = 5$ TeV, in order to satisfy the WMAP bounds [23]. Reaching far above the ω scale, the inert fields are highly degenerated, and the coannihilations such as $H_1'A_1'$, $H_1'H_2'$, $H_1'H_3'$, and so on, dominate over the effective annihilation cross section of dark matter. As a matter of fact, all the inert doublet and singlet components have gauge interactions with ordinary and new gauge bosons such that the s-channel coannihilation cross sections are turned on in this regime, which are more enhanced than the annihilation ones (this is also valid for the scalar interactions, but is not signified in that case). This effect makes the relic density continuously decrease [21]. The simple 3-3-1 model, like the minimal 3-3-1 model, encounters a low Landau pole [25]; the next evolution of dark-matter mass is therefore nonsense.

All the above conclusions are shown more clearly in Fig. 2, in which we determine the $\omega - \mu_{\eta'}$ (left) and $\omega - m_{H_1'}$ (right) planes by varying both ω and $\mu_{\eta'}$ in the regions (3000 GeV $< \omega <$ 9000 TeV) and (100 GeV $< \mu_{\eta'} <$ 3100 GeV). The color regions are in agreement with the requirement $\Omega h^2 < 0.1176$. The red regions satisfy $0.1064 < \Omega h^2 < 0.1176$. The lightest dark-matter mass can be at the electroweak scale, $m_{H_1'}(\text{min}) = 235.2$ GeV for $\omega = 3$ TeV and $\mu_{\eta'} = 100$ GeV. However, please note that this is by our choice of the parameter values, despite the fact that the dark matter has a natural mass in the ω scale, as mentioned before. The right panel of Fig. 2 shows that the 600-GeV dark matter supplies the correct relic density when ω changes (corresponding to the red point line in the region $\mu_{\eta'} < 600$ GeV in the left panel). This is due to the Standard Model contribution only. The middle (straight) red point line is due to the H resonance. The rightmost red point line is due to the contribution of new particles of the simple 3-3-1 model. Here, the dark-matter mass is beyond 1 TeV.

Now let us consider in detail the results of indirect and direct searches for dark matter. For example, with $\omega = 3$ TeV, $\mu_{\eta'} = 534$ GeV we get $m_{H_1'} = 574.7$ GeV and other inert particles $m_{H_2'} = 575.2$ GeV, $m_{A_1'} = 579.4$ GeV, and $m_{H_3'} = 831.2$ GeV. Since the mass-squared difference between $m^2_{H_1'}, m^2_{A_1'}$, and $m^2_{H_2'}$ is of the order of x_4u^2, x_6u^2, the mass of A_1' and $H_2'^{\pm}$ is very close to $m_{H_1'}$ for any values of ω. That is why the coannihilation contributes significantly to $\frac{1}{\Omega h^2}$. For the choice $\omega = 3$ TeV, $\mu_{\eta'} = 534$ GeV, we get $\Omega h^2 = 0.111$, and the main annihilation/coannihilation channels are

$$\begin{aligned} &H_2'^{+}H_2'^{-} \to W^+W^-, \qquad H_1'H_1' \to Z_1Z_1, \\ &H_1'H_1' \to W^+W^-, \qquad H_1'H_2'^{\pm} \to AW^{\pm}, \\ &H_2'^{+}H_2'^{-} \to AA. \end{aligned} \tag{25}$$

In this case, the photon flux, positron flux, and antiproton flux are

$$\begin{aligned} &2.8 \times 10^{-14}\ (\text{s cm}^2\,\text{sr GeV})^{-1}, \\ &1.8 \times 10^{-12}\ (\text{s cm}^2\,\text{sr GeV})^{-1}, \\ &3.5 \times 10^{-11}\ (\text{s cm}^2\,\text{sr GeV})^{-1}, \end{aligned}$$

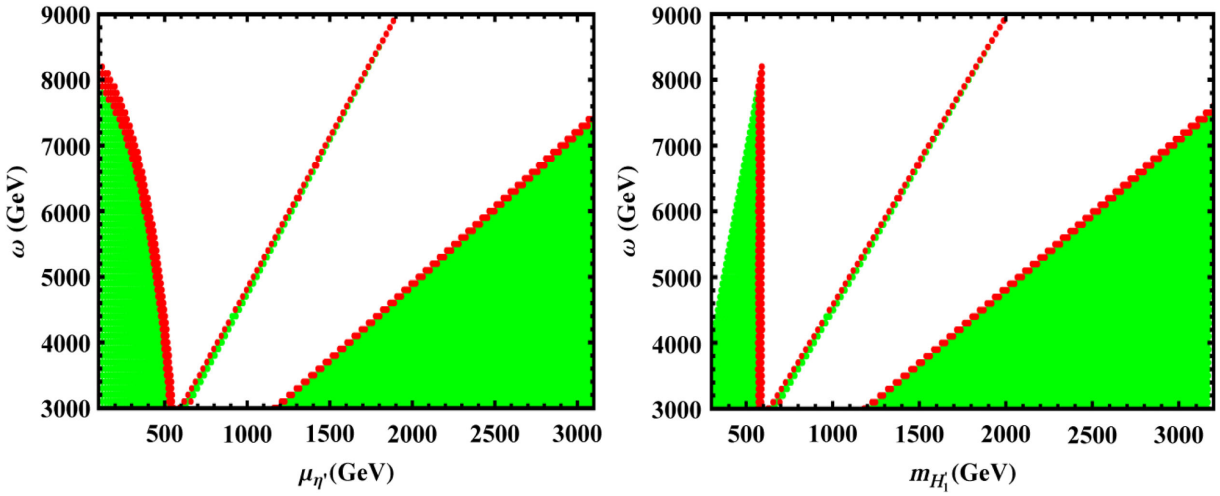

FIG. 2 (color online). Contour plot of the relic density on the ω-$\mu_{\eta'}$ plane (left) and the ω-$m_{H_1'}$ plane (right) in agreement with WMAP data. The red regions (in black and white, the darker fringe) yield the correct abundance, $0.1064 < \Omega h^2 < 0.1176$.

correspondingly, for the angle of sight 0.10 rad and energy $E = 100$ GeV. The $H_1' - p, n$ cross section is 1.5×10^{-47} cm^2 and the total number of events is 2.2×10^{-6} events/day/kg.

The dark-matter mass can be at the TeV scale if we choose $\mu_{\eta'} = 1171$ GeV for $\omega = 3$ TeV. In this case the dominant channels of annihilation/coannihilation can be heavy gauge bosons, such as $H_2'^{+}H_3'^{+} \to W^+X^+, Y^{++}Z_1$. For dark matter with mass around 570 GeV, the results of the relic density as well as the search for dark matter do not change when varying ω, since the couplings in the dominant channels do not depend on ω, as mentioned above. The plane $\langle\sigma.v_{\rm rel}\rangle - m_{H_1'}$ for the abundance below the experimental upper bound, $\Omega h^2(\max) = 0.1176$, is shown in Fig. 3. For the correct abundance of dark matter, the total annihilation cross section times the relative velocity of incoming dark-matter particles and the dark-matter mass is of the order of 10^{-26} cm^3/s for $m_{H_1'} < 2$ TeV, and it decreases when $m_{H_1'}$ increases because heavier dark matter increases the contribution of coannihilation to $\frac{1}{\Omega h^2}$.

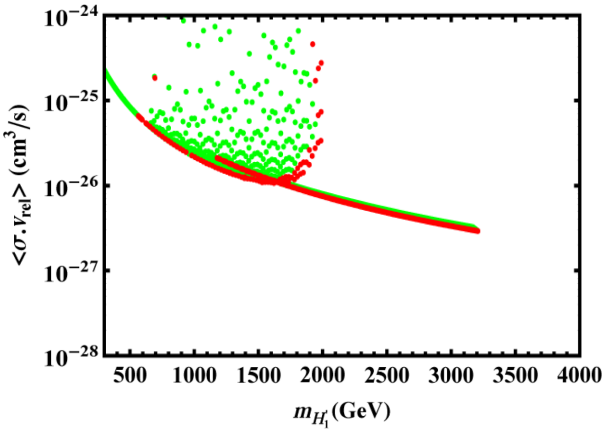

FIG. 3 (color online). The $\langle\sigma.v_{\rm rel}\rangle - m_{H_1'}$ plane in agreement with WMAP data. The red regions (in black and white, the darker regions) yield the correct abundance, $0.1064 < \Omega h^2 < 0.1176$.

Figure 4 shows the values of $\sigma_{\text{LIP-nucleon}}$ as a function of the dark-matter mass obtained from micrOMEGAs by fixing the nucleon form factors, $\sigma_0 = 30$ MeV and $\sigma_{\pi N} = 73$ MeV. The value of $\sigma_{\text{LIP-nucleon}}$ is 5.4×10^{-48} cm^2 for a Xe detector and the total number of events is 1.1×10^{-8} events/day/kg for dark matter with mass around 2 TeV.

Let us calculate the direct dark-matter search by hand and compare it to the results achieved from micrOMEGAs. The dark matter scatters off the nuclei of a large detector via interaction with quarks confined in nucleons. Because the dark matter is closely nonrelativistic, the process can be described by an effective Lagrangian [19],

$$\mathcal{L}_{\mathcal{S}} = 2\lambda_q m_{H_1'} H_1' H_1' \bar{q} q. \tag{26}$$

Note that for the real scalar field, only spin-independent and even interactions are possible. There exist interactions of the pair H_1' coupled to h and H_0. However, the dominant contributions to H_1'-quark scattering are done by the t-channel exchange of h. We obtain

$$\lambda_q = \frac{(x_2 + x_4 + x_6) m_q}{2 m_{H_1'} m_h^2}. \tag{27}$$

The H_1'-nucleon scattering amplitude is taken as a summation over the quark-level interactions with the respective nucleon form factors. The H_1'-nucleon cross section is given as

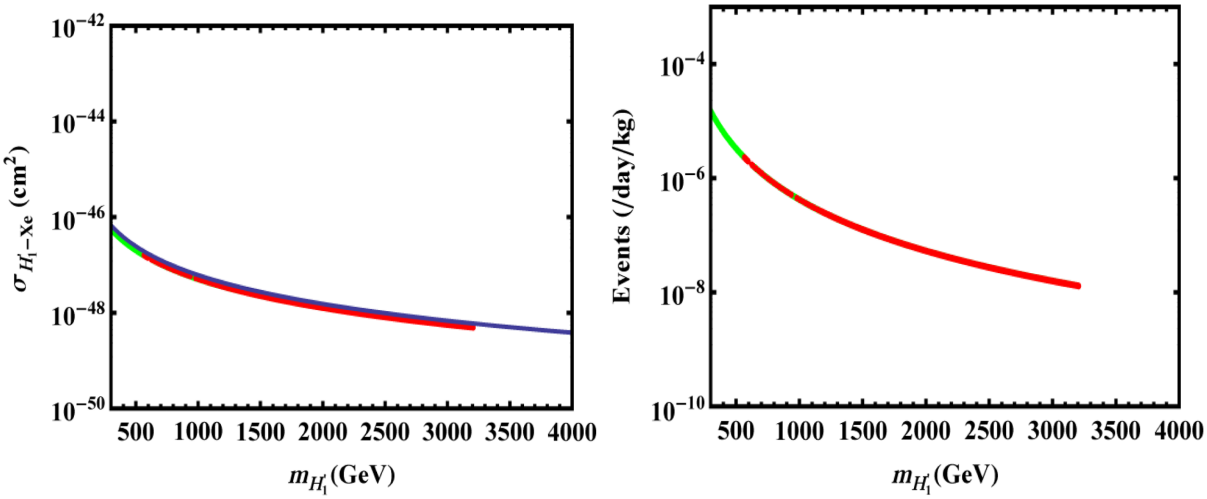

FIG. 4 (color online). $\sigma_{H_1'-N}$ (left) and the total number of events/day/kg (right) as functions of $m_{H_1'}$. The (blue) continuous line on the left panel was obtained from the analytical calculation for direct search.

$$\sigma_{H_1'-N} = \frac{4m_r^2}{\pi}\lambda_N^2, \tag{28}$$

where $N = p, n$ denotes nucleon, and

$$m_r = \frac{m_{H_1'} m_N}{m_{H_1'} + m_N} \simeq m_N,$$
$$\frac{\lambda_N}{m_N} = \sum_{u,d,s} f_{Tq}^N \frac{\lambda_q}{m_q} + \frac{2}{27} f_{TG}^N \sum_{c,b,t} \frac{\lambda_q}{m_q}, \tag{29}$$

where $f_{TG}^N = 1 - \sum_{u,d,s} f_{Tq}^N$. The f_{Tq}^N values were considered in [26],

$$f_{Tu}^N = 0.014 \pm 0.003, \qquad f_{Td}^N = 0.036 \pm 0.008,$$
$$f_{Ts}^N = 0.118 \pm 0.062. \tag{30}$$

Taking $m_N = 1$ GeV and $m_h = 125$ GeV [27], we obtain

$$\sigma_{H_1'-N} \simeq \left[\frac{(x_2 + x_4 + x_6)\ \text{TeV}}{m_{H_1'}}\right]^2 \times 6.146 \times 10^{-44}\ \text{cm}^2$$
$$\simeq \left[\frac{1\ \text{TeV}}{m_{H_1'}}\right]^2 \times 6.146 \times 10^{-48}\ \text{cm}^2, \tag{31}$$

noting that $x_{2,4,6}$ were given in Eq. (23). The $\sigma_{H_1'-N}$ obtained in Eq. (31) is inversely proportional to the square of the dark-matter mass that is shown as a (blue) continuous line passed by the red region in Fig. 4. It implies that the direct search calculated by hand is in nice agreement with the result yielded by the micrOMEGAs package.

Dark-matter candidates can be searched for at particle colliders as well. At the LHC, the collision of protons may produce candidates, recognized in form of large missing transverse momentum or energy. The minimal experimental signature would be an excess of a mono-X final state, recoiling against such missing energy. When H_1' is in the first region, its production is via the exchanges of the Standard Model h, Z, and W bosons, as it has couplings $hH_1'H_1'$, $ZH_1'A_1'$, $WH_1'H_2'$, $hhH_1'H_1'$, $ZZH_1'H_1'$, and $WWH_1'H_1'$ (note that h can interact with gluons via a t-quark loop). The mono-X signatures possibly include: (i) jet, which is either a gluon (g) or a quark (q), by processes $gg \to gH_1'H_1'$, $gq \to qH_1'H_1'$, $q\bar{q} \to gH_1'H_1'$ (all via h exchange), $gq \to qH_1'A_1'$, $q\bar{q} \to gH_1'A_1'$ (all via Z exchange), and $gq \to qH_1'H_2', q\bar{q} \to gH_1'H_2'$ (all via W exchange); (ii) $Z(W)$ by process $q\bar{q} \to Z(W)H_1'H_1'$ via $Z(W)$ and h (or only the former, without the latter) exchange; and (iii) h by processes $gg \to hH_1'H_1'$, $q\bar{q} \to hH_1'A_1'$ via h or $Z(W)$ exchange. Note that for the processes concerning the W boson, the two fields (q, q) do not mean the same quark. When H_1' is in the second or third region, the new physics of the 3-3-1 model contributes instead, where we have similar processes with h replaced by H and Z replaced by Z' (in this case, H interacts with gluons via exotic quark loops). The mono-X signatures are jet, Z', and H, possibly additionally including $H^\pm, X^\pm, Y^{\pm\pm}$, and exotic quarks. Data from LHC run I might provide some constraints, but the LHC run II would yield crucial tests of them. All the mentioned phenomena are worth exploring in future studies.

B. Dark matter in the simple 3-3-1 model with χ replication

The simple 3-3-1 model with χ replication contains six inert particles: $H_1'^\pm, H_2'^{\pm\pm}, H_3'$, and A_3'. If we assume that $y_6 < \min\{0, -y_5, (u/\omega)^2 y_4 - y_5\}$, H_3' is the lightest inert particle and can be the dark-matter candidate. The (co) annihilation processes concerning this candidate are given in Appendix C.

The parameters appeared in this model are $\mu_{\chi'}^2, \omega, \lambda_{1,2,3,4}$, and $y_{1,2,3,4,5,6}$, in which the couplings $\lambda_{1,2,3,4}$ are fixed as given in the η' model. Now let us consider the results for relic density and indirect search, as well as direct search with a set of $y_{1,2,3,4,5,6}$ in the same order,

$$y_1 = 0.01, \qquad y_2 = 0.04, \qquad y_3 = 0.058,$$
$$y_4 = 0.01, \qquad y_5 = 0.05, \qquad y_6 = -0.06. \tag{32}$$

All the ingredients of the simple 3-3-1 model, such as the masses of new particles, the mass hierarchies among the new particles and ordinary particles, and the couplings as given, are retained. Note also that the squared-mass splittings of inert fields are definitely small; the doublet components (H_1', H_2') are separated by the u scale, while the singlets H_3' and A_3', as well as the singlets and doublets, are separated by the ω scale.

Because the dark matter H_3' is a singlet under Standard Model symmetry, it does not have gauge interactions with Standard Model gauge bosons. Therefore, at low energy, the gauge portal for dark-matter (co)annihilations is suppressed. The relic density in this regime is only governed by the Higgs portal (h) with the Standard Model productions. The effective annihilation cross section times velocity is obtained by [10]

$$\langle \sigma v \rangle \simeq \left(\frac{\alpha}{150\ \text{GeV}}\right)^2 \left(\frac{y_2 \times 2.2\ \text{TeV}}{m_{H_3'}}\right)^2. \tag{33}$$

Because the chosen scalar coupling is small, $y_2 = 0.04$, the relic density given by $\Omega h^2 \simeq 0.1\ \text{pb}/\langle \sigma v \rangle \simeq 0.1 \times (m_{H_3'}/88\ \text{GeV})^2$ is overpopulated; this spoils the WMAP bounds, provided that $m_{H_3'}$ is larger than the weak scale. Of course, we can have a low-energy solution for the dark-matter candidate if the y_2 coupling is enhanced. While this possibility is interesting as studied in the literature [17], it will be not be addressed in our work. We are concerned with the high-energy regime of dark matter, where the simple 3-3-1 model contributions become important.

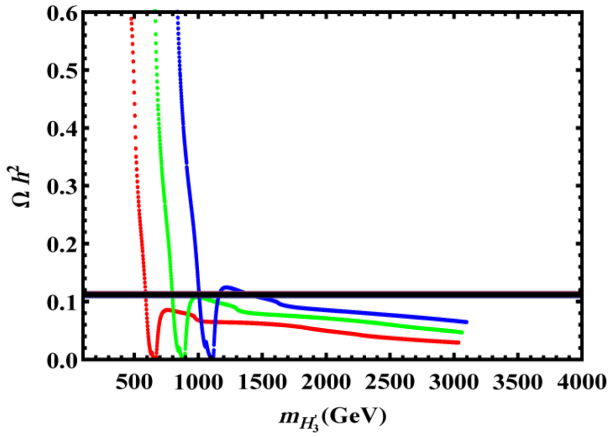

FIG. 5 (color online). Ωh^2 as a function of $m_{H_3'}$ for $\omega = 3$ TeV (red), $\omega = 4$ TeV (green), and $\omega = 5$ TeV (blue), from left to right, respectively.

The relic abundance is considered as a function of $m_{H_3'}$, shown in Fig. 5 for $\omega = 3$ TeV (red), $\omega = 4$ TeV (green), and $\omega = 5$ TeV (blue). For each value of ω, when the dark-matter mass rises from the outset, the relic density is rapidly decreased. This phenomenon is due to the H resonance of the dark-matter annihilation (H_3') into the Standard Model particles, including $H^{\pm}$ if kinematically allowed, analogous to the previous model. That is, the H resonance is crucial in determining the dark-matter relic density at its low-mass regime before new particles of the simple 3-3-1 model enter the production. The resonant point is given by $m_{H_3'} = \frac{1}{2} m_H$, which yields $m_{H_3'} \simeq 670$ GeV for $\omega = 3$ TeV, $m_{H_3'} \simeq 895$ GeV for $\omega = 4$ TeV, and $m_{H_3'} \simeq 1.118$ TeV for $\omega = 5$ TeV (these values coincide, respectively, with those of the previous model). Furthermore, the dark-matter mass is bounded by $m_{H_3'} \geq 580$ GeV for $\omega = 3$ TeV, $m_{H_3'} \geq 770$ GeV for $\omega = 4$ TeV, or $m_{H_3'} > 990$ GeV for $\omega = 5$ TeV.

After the resonant point, the relic density increases as the dark-matter mass increases. However, it is quickly depopulated due to the new contributions of the simple 3-3-1 model. From the figure we see that there is a gap (in the dark-matter mass) when $\omega > 4$ TeV; the relic density is overpopulated. The phenomenon happens in a similar manner as the previous model, because the dark-matter mass increases against the contributions from the new particles of the simple 3-3-1 model. Going far above the ω scale, the relic density still decreases. This effect is due to the large contributions of the coannihilations resulting from strongly degenerate inert fields [21]. Because the model has a low Landau pole, as mentioned [25], continuously rising the mass parameter is simply nonsense.

The discussion above can be illustrated more clearly in the $\omega - \mu_{\chi'}$ plane (left) and $\omega - m_{H_3'}$ plane (right) in Fig. 6. For each value of ω, there is a lower bound on the value of $\mu_{\chi'}$ that results in a respective lower bound on $m_{H_3'}$, in order to satisfy the WMAP data. It is different from the η' model in that the doublet dark matter H_1' in the η' model can appear near the electroweak scale as governed by the Standard Model gauge portal, but the singlet dark matter H_3' in the χ' model does not appear at this regime because the gauge portal does not work. Note that in this regime both models have suppressed Higgs portals. Given that the scalar couplings are enhanced (by other choices) in a comparable manner as the gauge couplings, their dark-matter phenomenologies should happen similarly. Again, from the figure, the two parallel red point lines at the leftmost regime present the edges of the resonant width imposed by WMAP bounds. The bottom of the red hat is the bound on ω ($\sim$4 TeV) at which the relic density becomes overpopulated after the resonance. The wide red bank describes various contributions of the new particles of the simple 3-3-1 model.

By varying ω and $\mu_{\chi'}$ in the ranges (3000, 9000) GeV and (100, 3000) GeV, respectively, we figure out the

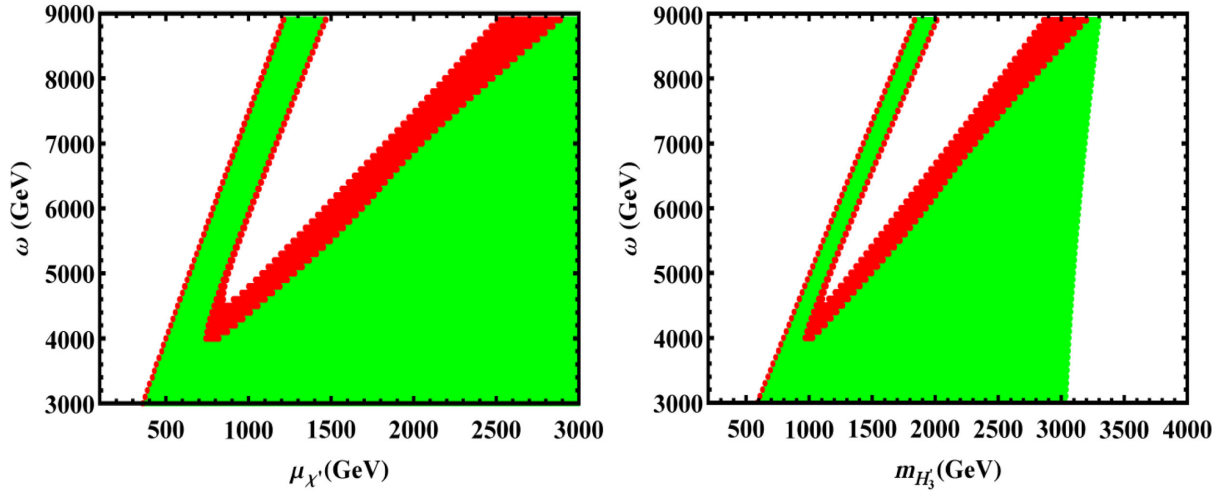

FIG. 6 (color online). Contour plot of the relic density on the $\omega - \mu_{\chi'}$ plane (left) and the $\omega - m_{H_3'}$ plane (right) in agreement with WMAP data. The red regions (in black and white, the darker fringe) yield the correct abundance, $0.1064 < \Omega h^2 < 0.1176$.

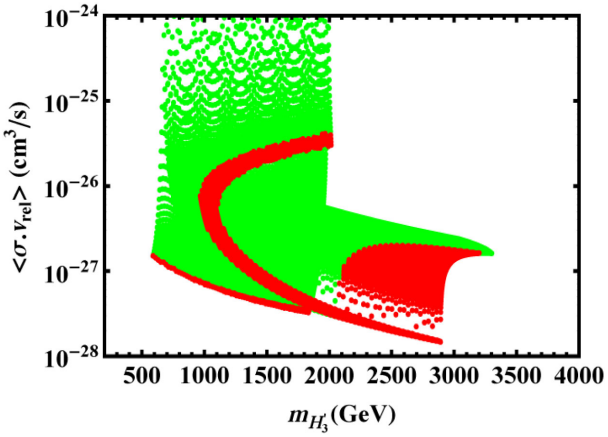

FIG. 7 (color online). The $\langle\sigma.v_{\rm rel}\rangle - m_{H_3'}$ plane in agreement with WMAP data. The red regions (in black and white, the darker regions) yield the correct abundance, $0.1064 < \Omega h^2 < 0.1176$.

$\langle\sigma.v_{\rm rel}\rangle - m_{H_3'}$ plane in Fig. 7, in which the green regions satisfy the relic density $\Omega h^2 \leq 0.1064$ while the red ones yield the correct abundance. The $\langle\sigma.v_{\rm rel}\rangle$ gets the typical value $\sim 10^{-26}$ cm^3/s for the dark-matter mass below 2 TeV, similar to the η' model. The direct search results depending on $m_{H_3'}$ are shown in Fig. 8. The H_3'-nucleon cross section is 2.1×10^{-47} cm^2 and the number of events is 8.7×10^{-7} events/day/kg for $m_{H_3'} = 2$ TeV.

Here, we give an example of dark matter at low energy. For $\omega = 3$ TeV, $\mu_{\chi'} = 361$ GeV, the dark matter with mass 589 GeV provides the abundance 0.11. The main annihilation/coannihilation channels are

$$H_3'H_3' \to hh, \quad H_2'^{++}H_2'^{--} \to hh, \quad H_1'^{+}H_1'^{-} \to hh,$$
$$H_3'H_1'^{\pm} \to Z_1X^{\pm}, \quad H_3'H_2'^{\pm\pm} \to Z_1Y^{\pm\pm}. \tag{34}$$

The photon flux, positron flux, and antiproton flux are

$$5.3 \times 10^{-16}\ (\text{s cm}^2\ \text{sr GeV})^{-1},$$
$$2.4 \times 10^{-14}\ (\text{s cm}^2\ \text{sr GeV})^{-1},$$
$$6.9 \times 10^{-13}\ (\text{s cm}^2\ \text{sr GeV})^{-1},$$

respectively, for the angle of sight 0.10 rad and energy $E = 100$ GeV. The $H_3' - p, n$ cross section is 2.3×10^{-46} cm^2 and the total number of events/day/kg is 3.3×10^{-5}. For the same dark-matter mass around 580 GeV, the signals in the indirect search for dark matter in the η' model are more sensitive, but the direct search results are lower, than that in the χ' model. This conclusion remains the same if we test for dark matter in the TeV range.

Similarly, we can calculate the direct search by hand as analysis of the η' model. The effective Lagrangian takes the form

$$\mathcal{L}'_{\mathcal{S}} = 2\lambda'_q m_{H_3'} H_3' H_3' \bar{q} q. \tag{35}$$

We obtain

$$\lambda'_q = \frac{y_2 m_q}{2 m_{H_3'} m_h^2}, \tag{36}$$

and finally

$$\sigma_{H_3'-N} \simeq \left[\frac{y_2\ \text{TeV}}{m_{H_3'}}\right]^2 \times 6.146 \times 10^{-44}\ \text{cm}^2. \tag{37}$$

The result given in Eq. (37) is depicted as a (blue) continuous line shown on the left side of Fig. 8 for $y_2 = 0.04$. The line goes through the red region, indicating that the result calculated by hand is in nice agreement with the one yielded from micrOMEGAs.

The mono-X search for H_3' differs from the previous case for the low-energy regime (if it is allowed by reselecting

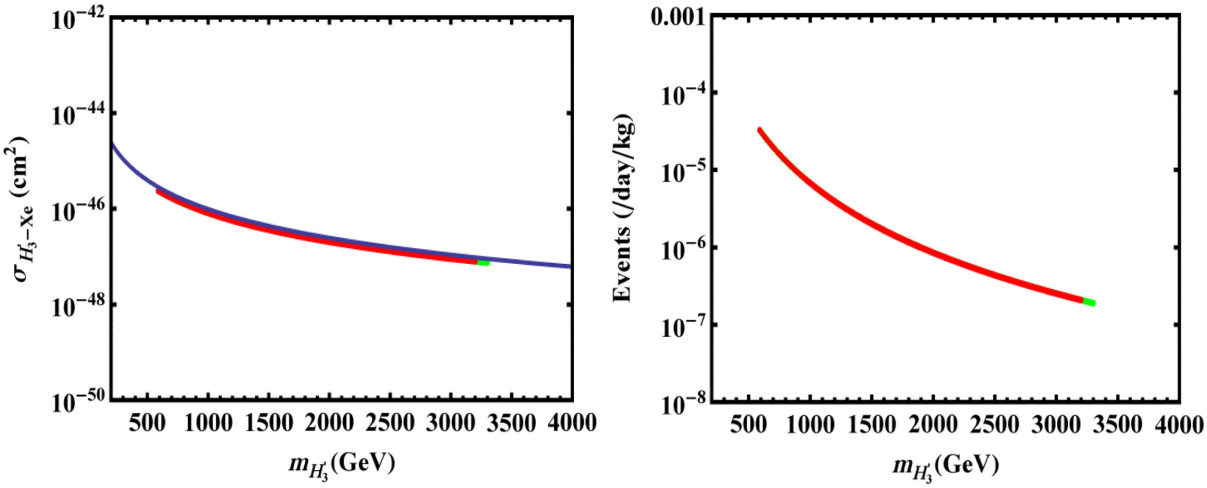

FIG. 8 (color online). $\sigma_{H_3'-N}$ (left) and the total number of events/day/kg (right) as functions of $m_{H_3'}$. The (blue) continuous line on the left panel was obtained from the analytical calculation for direct search.

parameter values) because it has only the Standard Model Higgs portal interactions. Therefore, only the processes that are exchanged by h are available. When H_3' is at the high-energy regime with the 3-3-1 contributions, the mono-X signatures are jet, H, and Z', and possibly include exotic quarks, $H^{\pm}$, $X^{\pm}$, and $Y^{\pm\pm}$. Here, all the processes analogous to the previous case are present. Therefore, the inert scalar singlet has rich phenomenologies featured for the 3-3-1 model, unlike previous proposals. Also, because this particle is bilepton, the new charged scalars $H^{\pm}$ might present characteristic signatures at colliders, and it can be created in pairs or in association with other bileptons such as the exotic quarks and new non-Hermitian gauge bosons.

IV. CONCLUSION

The minimal 3-3-1 model can work as the simple 3-3-1 model with two scalar triplets η and χ, while leaving all other scalars as odd (inert) fields under a Z_2 symmetry [11]. As a common feature of the 3-3-1 models recently investigated, the simple 3-3-1 model is only a low-energy effective theory such that $B-L$ nonconserving interactions must present [9,10]. This feature is strongly supported by the fact that the proton decay operator always disappears due to the lepton-party $(-1)^L$ conservation, while the small neutrino masses result from the approximate lepton-number symmetry [11]. Furthermore, with such criteria, inert fields as mentioned are naturally accommodated. Indeed, their presence (besides the neutrino mass operators) not only makes the model viable, but it also provides dark-matter candidates. The $B-L$ nonconserving interactions between inert fields and normal scalars are crucial to determine the dark-matter mass splitting from its complex counterpart. As a result, this splitting suppresses the large scattering magnitudes of dark matter with nuclei via the Z, Z' boson exchanges (which evades the strengthened direct search bounds). Among the inert fields proposed, the simple 3-3-1 model with inert $X=1$ sextet, the model with η replication (the η' model), and the version with χ replication (the χ' model) satisfy the above conditions. The latter two models have been further discussed in this work.

As a matter of fact, the original simple 3-3-1 model does not contain dark matter. The introduction of inert triplets (η' in the η' model and χ' in the χ' model) that are odd under a Z_2 symmetry (where all the other fields are even) means that they do not mix with normal particles. Because of the Z_2 conservation, inert scalars have zero VEV and interact only with the normal scalars and gauge bosons. There is no interaction between inert particles and fermions. The lightest and neutral inert particle is stable; it can be the dark-matter candidate. Our proposals provide a doublet dark matter H_1', in the η' model, as well as a singlet dark matter H_3', in the χ' model. All the relevant interactions that can contribute to the annihilation/coannihilation processes have been calculated. The results for the relic density as well as experimental searches for the dark-matter candidates have been investigated using the micrOMEGAs package including the implementation of the new model files.

It is interesting that in both the η' and χ' models, the dark-matter observables in the middle scale (between the weak and 3-3-1 scales) are governed by the H resonance, where H is the new neutral Higgs boson of the simple 3-3-1 model. The dominant contributions from various new gauge portals and the new Higgs portal set the dark-matter observables in the 3-3-1 scale. The large coannihilation effects due to strongly degenerated inert fields make the relic densities continuously decrease when the dark-matter masses are very large, far above the ω scale. There is a limit for the dark-matter mass, as well as the dark-matter observables, due to the Landau pole subjected to the 3-3-1 models. At low energy, the doublet candidate H_1' has the Standard Model gauge portal interactions, whereas the singlet one H_3' does not. Both candidates can interact with the Standard Model via the Higgs portal (h). If the scalar couplings for the candidates are small in comparison to the gauge couplings, there is no low-energy solution for the singlet candidate. However, when the scalar couplings become comparable to the gauge ones, all of them can be realized as low-energy dark matters via the Higgs portal language.

From the imposed parameter values, the following conclusions are derived:

(1) The region below 2 TeV yields the typical value of the thermally averaged annihilation cross section times velocity for dark matter, $\langle\sigma v\rangle \sim 10^{-26}$ cm^3/s.
(2) The dark matter–nucleon scattering cross section given by micrOMEGAs perfectly coincides with the theoretical computation. Furthermore, the values achieved are in agreement with the experimental data.
(3) For each value of ω, the dark-matter mass region that yields the correct abundance is quite narrow.
(4) For all values of ω, the doublet dark matter H_1' in the η' model can be at the electroweak scale, up to the scale bounded by 600 GeV. The singlet dark matter H_3' in the χ' model disappears in this range. There is a lower bound on $m_{H_3'}$, for example, $m_{H_3'} > 580$ GeV for $\omega = 3$ TeV, $m_{H_3'} > 770$ GeV for $\omega = 4$ TeV, or $m_{H_3'} > 990$ GeV for $\omega = 5$ TeV.
(5) Both models have same resonance point at the middle scale, $m_{\rm DM} = \frac{1}{2} m_H$: $m_{\rm DM} \simeq 670$ GeV for $\omega = 3$ TeV, $m_{\rm DM} \simeq 895$ GeV for $\omega = 4$ TeV, and $m_{\rm DM} \simeq 1.118$ TeV for $\omega = 5$ TeV.
(6) The indirect search (the particle fluxes) for the dark-matter candidate in the η' model is more sensitive. However, the direct search results such as the $\sigma_{\text{LIP-nucleon}}$, the total number of events/day/kg, are lower for the same dark-matter mass in comparison with signals in the χ' model.

With the results obtained, we first conclude that the 3-3-1 models may have a natural room for dark matter, and

second, that the dark-matter phenomenologies are rich. All of our results call for further study.

ACKNOWLEDGMENTS

This research is funded by Vietnam National Foundation for Science and Technology Development (NAFOSTED) under Grant No. 103.01-2013.43, and by the National Research Foundation of Korea (NRF) funded by the Ministry of Education, Science and Technology (MEST) of the government of Korea (Grants No. 2011-0017430 and No. 2011-0020333).

APPENDIX A: INTERACTIONS OF INERT AND NORMAL SECTORS IN THE η' MODEL

The Higgs boson–inert scalar interactions are obtained by expanding the $V_{\eta'}$ as follows:

$$
\begin{aligned}
V_{\eta'} \supset\ & x_1\left[\frac{1}{2}(H_1'^2+A_1'^2)+H_2'^+H_2'^-+H_3'^+H_3'^-\right]^2+x_2\left[\frac{1}{2}(u+h)^2+H^+H^-\right]\times\left[\frac{1}{2}(H_1'^2+A_1'^2)+H_2'^+H_2'^-+H_3'^+H_3'^-\right]\\
&+\frac{x_3}{2}(\omega+H)^2\times\left[\frac{1}{2}(H_1'^2+A_1'^2)+H_2'^+H_2'^-+H_3'^+H_3'^-\right]\\
&+x_4\left[\frac{1}{2}(u+h)(H_1'+iA_1')+H_3'^+H^-\right]\times\left[\frac{1}{2}(u+h)(H_1'-iA_1')+H^+H_3'^-\right]\\
&+\frac{x_5}{2}(\omega+H)^2H_3'^+H_3'^-+\frac{1}{2}x_6\left[\left[\frac{1}{2}(u+h)(H_1'-iA_1')\right]^2+(H_3'^-H^+)^2+\text{H.c.}\right].
\end{aligned}
\tag{A1}
$$

All the interactions of inert scalars with normal Higgs bosons are listed in Table I. Note that the symmetry factor and imaginary unit as imposed by the Feynman rules are not included in the tables (the interacting Lagrangian is understood as the coupling multiplied by the vertex, respectively).

The triple interactions of the two inert scalars with one gauge boson are given in

$$
\begin{aligned}
\mathcal{L}^{\text{triple}}_{\text{gauge}-\eta'} &= -ig[\eta'^\dagger(T_iA_{i\mu})\partial^\mu\eta'] + \text{H.c.}\\
&= -\frac{ig}{2}\left[\frac{1}{c_W}Z_{1\mu}+\sqrt{\frac{1-3t_W^2}{3}}Z_{2\mu}\right]\frac{H_1'-iA_1'}{\sqrt{2}}\overset{\leftrightarrow\mu}{\partial}\frac{H_1'+iA_1'}{\sqrt{2}}-\frac{ig}{2}\left[-2s_WA_\mu-\frac{c_{2W}}{c_W}Z_{1\mu}+\sqrt{\frac{1-3t_W^2}{3}}Z_{2\mu}\right]H_2'^+\overset{\leftrightarrow\mu}{\partial}H_2'^-\\
&\quad -ig\left[s_WA_\mu-s_Wt_WZ_{1\mu}-\sqrt{\frac{1-3t_W^2}{3}}Z_{2\mu}\right]H_3'^-\overset{\leftrightarrow\mu}{\partial}H_3'^+\\
&\quad -\frac{ig}{2}[W_\mu^+(H_1'-iA_1')\overset{\leftrightarrow\mu}{\partial}H_2'^-+X_\mu^-(H_1'-iA_1')\overset{\leftrightarrow\mu}{\partial}H_3'^++\sqrt{2}Y_\mu^{--}H_2'^+\overset{\leftrightarrow\mu}{\partial}H_3'^++\text{H.c.}],
\end{aligned}
\tag{A2}
$$

where we have denoted $A\overset{\leftrightarrow\mu}{\partial}B=A(\partial^\mu B)-(\partial^\mu A)B$.

The quartic interactions of the two inert scalars with two gauge bosons are given by

$$
\begin{aligned}
\mathcal{L}^{\text{quartic}}_{\text{gauge}-\eta'} &= g^2[\eta'^\dagger(T_iA_{i\mu})^2\eta']\\
&= \frac{g^2}{4}\left[W^{+\mu}W_\mu^-+X^{+\mu}X_\mu^-+\frac{1}{2}\left(\frac{1}{c_W}Z_{1\mu}+\frac{\sqrt{1-3t_W^2}}{\sqrt{3}}Z_{2\mu}\right)^2\right](H_1'^2+A_1'^2)\\
&\quad +\frac{g^2}{4}\left[2W^{+\mu}W_\mu^-+2Y^{++\mu}Y_\mu^{--}+\left(2s_WA_\mu+\frac{c_{2W}}{c_W}Z_{1\mu}-\frac{\sqrt{1-3t_W^2}}{\sqrt{3}}Z_{2\mu}\right)^2\right]H_2'^+H_2'^-\\
&\quad +\frac{g^2}{4}\left[2X^{+\mu}X_\mu^-+2Y^{++\mu}Y_\mu^{--}+4\left(s_WA_\mu+s_Wt_WZ_{1\mu}+\frac{\sqrt{1-3t_W^2}}{\sqrt{3}}Z_{2\mu}\right)^2\right]H_3'^+H_3'^-\\
&\quad +\frac{g^2}{4}\left[\left(\sqrt{2}X^{-\mu}Y_\mu^{++}+2W^{+\mu}\left(-s_WA_\mu+s_Wt_WZ_{1\mu}+\frac{\sqrt{1-3t_W^2}}{\sqrt{3}}Z_{2\mu}\right)\right)(H_1'-iA_1')H_2'^-+\text{H.c.}\right]\\
&\quad +\frac{g^2}{4}\left[\left(\sqrt{2}W^{+\mu}Y_\mu^{--}+X^{-\mu}\left(2s_WA_\mu+\frac{c_{2W}}{c_W}Z_{1\mu}-\frac{\sqrt{1-3t_W^2}}{\sqrt{3}}Z_{2\mu}\right)\right)(H_1'-iA_1')H_3'^++\text{H.c.}\right]\\
&\quad +\frac{g^2}{4}\left[\left(2W^{-\mu}X_\mu^--\sqrt{2}Y^{--\mu}\left(\frac{1}{c_W}Z_{1\mu}+\frac{\sqrt{1-3t_W^2}}{\sqrt{3}}Z_{2\mu}\right)\right)H_2'^+H_3'^++\text{H.c.}\right].
\end{aligned}
\tag{A3}
$$

All the triple and quartic interactions of inert scalars with gauge bosons are presented in Table II and Table III, respectively.

TABLE I. Interactions of inert scalars with normal Higgs bosons in the η' model.

Vertex	Coupling	Vertex	Coupling
$hA_1'A_1'$	$\frac{(x_2+x_4-x_6)u}{2}$	$hH_1'H_1'$	$\frac{(x_2+x_4+x_6)u}{2}$
$hH_2'^+H_2'^-$	x_2u	$hH_3'^+H_3'^-$	x_2u
$HA_1'A_1'$	$\frac{x_3\omega}{2}$	$HH_1'H_1'$	$\frac{x_3\omega}{2}$
$HH_2'^+H_2'^-$	$x_3\omega$	$HH_3'^+H_3'^-$	$(x_3+x_5)\omega$
$H_1'H^+H_3'^-$	$\frac{(x_4+x_6)u}{2}$	$A_1'H_3'^+H^-$	$\frac{i(x_6-x_4)u}{2}$
$H_1'H_1'hh$	$\frac{x_2+x_4+x_6}{4}$	$H_1'H_1'H^+H^-$	$\frac{x_2}{2}$
$H_1'H_1'HH$	$\frac{x_3}{4}$	$H_1'H_1'A_1'A_1'$	$\frac{x_1}{2}$
$A_1'A_1'H^+H^-$	$\frac{x_2}{2}$	$A_1'A_1'HH$	$\frac{x_3}{4}$
$A_1'A_1'hh$	$\frac{x_2+x_4-x_6}{4}$	$A_1'A_1'H_2'^+H_2'^-$	x_1
$A_1'A_1'H_3'^+H_3'^-$	x_1	$H_1'H_3'^+H^-h$	$\frac{x_4+x_6}{2}$
$A_1'H_3'^+H^-h$	$\frac{i(x_6-x_4)}{2}$	$H_1'H_1'H_2'^+H_2'^-$	x_1
$hhH_2'^+H_2'^-$	$\frac{x_2}{2}$	$HHH_2'^+H_2'^-$	$\frac{x_3}{2}$
$H^+H^-H_2'^+H_2'^-$	x_2	$H_2'^+H_2'^-H_3'^+H_3'^-$	$2x_1$
$H_1'H_1'H_3'^+H_3'^-$	x_1	$hhH_3'^+H_3'^-$	$\frac{x_2}{2}$
$HHH_3'^+H_3'^-$	$\frac{x_3+x_5}{2}$	$H^+H^-H_3'^+H_3'^-$	x_2+x_4

TABLE II. Triple interactions of inert scalars with gauge bosons in the η' model.

Vertex	Coupling	Vertex	Coupling
$Z_{1\mu}H_1'\overleftrightarrow{\partial^\mu}A_1'$	$\frac{g}{2c_W}$	$Z_{2\mu}H_1'\overleftrightarrow{\partial^\mu}A_1'$	$\frac{g\sqrt{1-4s_W^2}}{2\sqrt{3}c_W}$
$W_\mu^-H_1'\overleftrightarrow{\partial^\mu}H_2'^+$	$\frac{ig}{2}$	$X_\mu^-H_1'\overleftrightarrow{\partial^\mu}H_3'^+$	$-\frac{ig}{2}$
$W_\mu^+A_1'\overleftrightarrow{\partial^\mu}H_2'^-$	$-\frac{g}{2}$	$X_\mu^+A_1'\overleftrightarrow{\partial^\mu}H_3'^-$	$-\frac{g}{2}$
$A_\mu H_2'^+\overleftrightarrow{\partial^\mu}H_2'^-$	igs_W	$Y_\mu^{--}H_2'^+\overleftrightarrow{\partial^\mu}H_3'^+$	$-\frac{ig}{\sqrt{2}}$
$Z_{1\mu}H_2'^+\overleftrightarrow{\partial^\mu}H_2'^-$	$\frac{igc_{2W}}{2c_W}$	$Z_{2\mu}H_2'^+\overleftrightarrow{\partial^\mu}H_2'^-$	$-\frac{ig\sqrt{1-4s_W^2}}{2\sqrt{3}c_W}$
$A_\mu H_3'^+\overleftrightarrow{\partial^\mu}H_3'^-$	igs_W	$Z_{1\mu}H_3'^+\overleftrightarrow{\partial^\mu}H_3'^-$	$-igs_Wt_W$
$Z_{2\mu}H_3'^+\overleftrightarrow{\partial^\mu}H_3'^-$	$-\frac{ig\sqrt{1-4s_W^2}}{\sqrt{3}c_W}$		

TABLE III. Quartic interactions of inert scalars with gauge bosons in the η' model.

Vertex	Coupling	Vertex	Coupling
$H_1'H_1'W^+W^-$	$\frac{g^2}{4}$	$H_1'H_1'X^+X^-$	$\frac{g^2}{4}$
$H_1'H_1'Z_1Z_1$	$\frac{g^2}{8c_W^2}$	$H_1'H_1'Z_1Z_2$	$\frac{g^2\sqrt{1-4s_W^2}}{4\sqrt{3}c_W^2}$
$H_1'H_1'Z_2Z_2$	$\frac{g^2(1-4s_W^2)}{24c_W^2}$	$A_1'A_1'W^+W^-$	$\frac{g^2}{4}$
$A_1'A_1'X^+X^-$	$\frac{g^2}{4}$	$A_1'A_1'Z_1Z_1$	$\frac{g^2}{8c_W^2}$
$A_1'A_1'Z_1Z_2$	$\frac{g^2\sqrt{1-4s_W^2}}{4\sqrt{3}c_W^2}$	$A_1'A_1'Z_2Z_2$	$\frac{g^2(1-4s_W^2)}{24c_W^2}$
$H_1'H_2'^+AW^-$	$-\frac{g^2s_W}{2}$	$H_1'H_2'^+X^+Y^{--}$	$\frac{g^2}{2\sqrt{2}}$
$H_1'H_2'^+Z_1W^-$	$\frac{g^2s_Wt_W}{2}$	$H_1'H_2'^+Z_2W^-$	$\frac{g^2\sqrt{1-4s_W^2}}{2\sqrt{3}c_W}$
$H_1'H_3'^+AX^-$	$\frac{g^2s_W}{2}$	$H_1'H_3'^+W^+Y^{--}$	$\frac{g^2}{2\sqrt{2}}$
$H_1'H_3'^+Z_1X^-$	$\frac{g^2c_{2W}}{4c_W}$	$H_1'H_3'^+Z_2X^-$	$-\frac{g^2\sqrt{1-4s_W^2}}{4\sqrt{3}c_W}$
$A_1'H_2'^+AW^-$	$-\frac{ig^2s_W}{2}$	$A_1'H_2'^+X^+Y^{--}$	$\frac{ig^2}{2\sqrt{2}}$
$A_1'H_2'^+Z_1W^-$	$\frac{ig^2s_Wt_W}{2}$	$A_1'H_2'^+Z_2W^-$	$\frac{ig^2\sqrt{1-4s_W^2}}{2\sqrt{3}c_W}$
$A_1'H_3'^+AX^-$	$-\frac{ig^2s_W}{2}$	$A_1'H_3'^+W^+Y^{--}$	$-\frac{ig^2}{2\sqrt{2}}$
$A_1'H_3'^+Z_1X^-$	$-\frac{ig^2c_{2W}}{4c_W}$	$A_1'H_3'^+Z_2X^-$	$\frac{ig^2\sqrt{1-4s_W^2}}{4\sqrt{3}c_W}$
$H_2'^+H_2'^-AA$	$g^2s_W^2$	$H_2'^+H_2'^-AZ_1$	$g^2c_{2W}t_W$
$H_2'^+H_2'^-AZ_2$	$-\frac{g^2t_W\sqrt{1-4s_W^2}}{\sqrt{3}}$	$H_2'^+H_2'^-W^+W^-$	$\frac{g^2}{2}$
$H_2'^+H_2'^-Y^{++}Y^{--}$	$\frac{g^2}{2}$	$H_2'^+H_2'^-Z_1Z_1$	$\frac{g^2c_{2W}^2}{4c_W^2}$
$H_2'^+H_2'^-Z_1Z_2$	$-\frac{g^2c_{2W}\sqrt{1-4s_W^2}}{2\sqrt{3}c_W^2}$	$H_2'^+H_2'^-Z_2Z_2$	$\frac{g^2(1-4s_W^2)}{12c_W^2}$
$H_3'^+H_3'^-AA$	$g^2s_W^2$	$H_3'^+H_3'^-AZ_1$	$-2g^2s_W^2t_W$
$H_3'^+H_3'^-AZ_2$	$-\frac{2g^2t_W\sqrt{1-4s_W^2}}{\sqrt{3}}$	$H_3'^+H_3'^-X^+X^-$	$\frac{g^2}{2}$
$H_3'^+H_3'^-Y^{++}Y^{--}$	$\frac{g^2}{2}$	$H_3'^+H_3'^-Z_1Z_1$	$\frac{g^2s_W^4}{c_W^2}$
$H_3'^+H_3'^-Z_1Z_2$	$\frac{2g^2t_W^2\sqrt{1-4s_W^2}}{\sqrt{3}}$	$H_3'^+H_3'^-Z_2Z_2$	$\frac{g^2(1-4s_W^2)}{3c_W^2}$

APPENDIX B: INTERACTIONS OF INERT AND NORMAL SECTORS IN THE χ' MODEL

The Higgs boson-inert scalar interactions are obtained as follows:

$$
\begin{aligned}
V_{\chi'} \supset\ & y_1\left[H_1'^+H_1'^- + H_2'^{++}H_2'^{--} + \frac{1}{2}(H_3'^2 + A_3'^2)\right]^2 \\
& + y_2\left[\frac{(u+h)^2}{2} + H^+H^-\right] \times \left[H_1'^+H_1'^- + H_2'^{++}H_2'^{--} + \frac{1}{2}(H_3'^2 + A_3'^2)\right] \\
& + \frac{y_3}{2}(\omega+H)^2 \times \left[H_1'^+H_1'^- + H_2'^{++}H_2'^{--} + \frac{1}{2}(H_3'^2 + A_3'^2)\right] \\
& + \frac{y_4}{2}[(u+h)H_1'^- + (H_3' + iA_3')H^-] \times [(u+h)H_1'^+ + (H_3' - iA_3')H^+] \\
& + \frac{1}{4}(\omega+H)^2[(y_5+y_6)H_3'^2 + (y_5-y_6)A_3'^2].
\end{aligned}
\tag{B1}
$$

TABLE IV. Interactions of inert scalars with normal Higgs bosons in the χ' model.

Vertex	Coupling	Vertex	Coupling
$hH'_3H'_3$	$\frac{y_2 u}{2}$	$hA'_3A'_3$	$\frac{y_2 u}{2}$
$hH'^+_1H'^-_1$	$(y_2+y_4)u$	$hH'^{++}_2H'^{--}_2$	$y_2 u$
$HH'_3H'_3$	$\frac{(y_3+y_5+y_6)\omega}{2}$	$HA'_3A'_3$	$\frac{(y_3+y_5-y_6)\omega}{2}$
$HH'^+_1H'^-_1$	$y_3\omega$	$HH'^{++}_2H'^{--}_2$	$y_3\omega$
$H'_3H^-H'^+_1$	$\frac{y_4 u}{2}$	$A'_3H^-H'^+_1$	$\frac{iy_4 u}{2}$
$H'_3H'_3hh$	$\frac{y_2}{4}$	$H'_3H'_3H^+H^-$	$\frac{y_2+y_4}{2}$
$H'_3H'_3HH$	$\frac{y_3+y_5+y_6}{4}$	$H'_3H'_3A'_3A'_3$	$\frac{y_1}{2}$
$H'_3H'_3H'^+_1H'^-_1$	y_1	$H'_3H'_3H'^{++}_2H'^{--}_2$	y_1
$A'_3A'_3H^+H^-$	$\frac{y_2+y_4}{2}$	$A'_3A'_3HH$	$\frac{y_3+y_5-y_6}{4}$
$A'_3A'_3hh$	$\frac{y_2}{4}$	$A'_3A'_3H'^+_1H'^-_1$	y_1
$A'_3A'_3H'^{++}_2H'^{--}_2$	y_1	$H'_3H'^+_1H^-h$	$\frac{y_4}{2}$
$A'_3H'^+_1H^-h$	$\frac{iy_4}{2}$	$hhH'^+_1H'^-_1$	$\frac{y_2+y_4}{2}$
$HHH'^+_1H'^-_1$	$\frac{y_3}{2}$	$H^+H^-H'^+_1H'^-_1$	y_2
$H'^+_2H'^-_2H'^+_1H'^-_1$	$2y_1$	$hhH'^{++}_2H'^{--}_2$	$\frac{y_2}{2}$
$HHH'^{++}_2H'^{--}_2$	$\frac{y_3}{2}$	$H^+H^-H'^{++}_2H'^{--}_2$	y_2

Interactions of two inert scalars with one gauge boson are shown in

$$\begin{aligned}\mathcal{L}^{\text{triple}}_{\text{gauge}-\chi'} &= -ig[\chi'^\dagger(T_iA_{i\mu}-tB_\mu I)\partial^\mu\chi'] \\ &= -\frac{ig}{2}\left[-2s_WA_\mu+\frac{1+2s_W^2}{c_W}Z_{1\mu}+\frac{1-9t_W^2}{\sqrt{3}\sqrt{1-3t_W^2}}Z_{2\mu}\right]H'^+_1\overleftrightarrow{\partial}^\mu H'^-_1 \\ &\quad -\frac{ig}{2}\left[-4s_WA_\mu-c_W(1-3t_W^2)Z_{1\mu}+\frac{1-9t_W^2}{\sqrt{3}\sqrt{1-3t_W^2}}Z_{2\mu}\right]H'^{++}_2\overleftrightarrow{\partial}^\mu H'^{--}_2+ig\left[\frac{1}{\sqrt{3}\sqrt{1-3t_W^2}}Z_{2\mu}\right]\frac{H'_3-iA'_3}{\sqrt{2}}\overleftrightarrow{\partial}^\mu\frac{H'_3+iA'_3}{\sqrt{2}} \\ &\quad -\frac{ig}{\sqrt{2}}\left[W^+_\mu H'^+_1\overleftrightarrow{\partial}^\mu H'^{--}_2+X^+_\mu\frac{H'_3-iA'_3}{\sqrt{2}}\overleftrightarrow{\partial}^\mu H'^-_1+Y^{++}_\mu\frac{H'_3-iA'_3}{\sqrt{2}}\overleftrightarrow{\partial}^\mu H'^{--}_2+\text{H.c.}\right]. \end{aligned} \tag{B2}$$

Quartic interactions of two inert scalars with two gauge bosons are given by

$$\begin{aligned}\mathcal{L}^{\text{quartic}}_{\text{gauge}-\chi'} &= g^2[\chi'^\dagger(T_iA_{i\mu}-tB_\mu I)^2\chi'] \\ &= \frac{g^2}{2}(W^{+\mu}W^-_\mu+X^{+\mu}X^-_\mu)H'^+_1H'^-_1+\frac{g^2}{2}(W^{+\mu}W^-_\mu+Y^{++\mu}Y^{--}_\mu)H'^{++}_2H'^{--}_2 \\ &\quad +\frac{g^2}{4}\left(-2s_WA_\mu+\frac{1+2s_W^2}{c_W}Z_{1\mu}+\frac{1-9t_W^2}{\sqrt{3}\sqrt{1-3t_W^2}}Z_{2\mu}\right)^2H'^+_1H'^-_1 \\ &\quad +\frac{g^2}{4}\left(4s_WA_\mu+c_W(1-3t_W^2)Z_{1\mu}-\frac{1-9t_W^2}{\sqrt{3}\sqrt{1-3t_W^2}}Z_{2\mu}\right)^2H'^{++}_2H'^{--}_2 \\ &\quad +\frac{g^2}{4}\left[X^{+\mu}X^-_\mu+Y^{++\mu}Y^{--}_\mu+\frac{2}{3(1-3t_W^2)}Z'^\mu_2Z_{2\mu}\right](H'^2_3+A'^2_3) \\ &\quad +\frac{g^2}{4}\left[2\left(X^{-\mu}Y^{++}_\mu+\sqrt{2}W^{+\mu}\left[-3s_WA_\mu+3s_Wt_WZ_{1\mu}+\frac{1-9t_W^2}{\sqrt{3}\sqrt{1-3t_W^2}}Z_{2\mu}\right]\right)H'^+_1H'^{--}_2\right. \\ &\quad +\left(\sqrt{2}W^{+\mu}Y^{--}_\mu+X^{-\mu}\left[-2s_WA_\mu+\frac{1+2s_W^2}{c_W}Z_{1\mu}-\frac{1+9t_W^2}{\sqrt{3}\sqrt{1-3t_W^2}}Z_{2\mu}\right]\right)H'^+_1(H'_3+iA'_3) \\ &\quad \left.+\left(\sqrt{2}W^{-\mu}X^-_\mu+Y^{--\mu}\left[-4s_WA_\mu-c_W(1-3t_W^2)Z_{1\mu}-\frac{1+9t_W^2}{\sqrt{3}\sqrt{1-3t_W^2}}Z_{2\mu}\right]\right)H'^{++}_2(H'_3+iA'_3)+\text{H.c.}\right]. \end{aligned} \tag{B3}$$

TABLE V. Triple interactions of inert scalars with gauge bosons in the χ' model.

Vertex	Coupling	Vertex	Coupling
$Z_{2\mu}H_3'\overleftrightarrow{\partial}^{\mu}A_3'$	$-\frac{gc_W}{\sqrt{3}\sqrt{1-4s_W^2}}$	$X_\mu^+H_3'\overleftrightarrow{\partial}^{\mu}H_1'^-$	$-\frac{ig}{2}$
$Y_\mu^{++}H_3'\overleftrightarrow{\partial}^{\mu}H_2'^{--}$	$-\frac{ig}{2}$	$X_\mu^+A_3'\overleftrightarrow{\partial}^{\mu}H_1'^-$	$-\frac{g}{2}$
$Y_\mu^{++}A_3'\overleftrightarrow{\partial}^{\mu}H_2'^{--}$	$-\frac{g}{2}$	$A_\mu H_1'^+\overleftrightarrow{\partial}^{\mu}H_1'^-$	igs_W
$W_\mu^+H_1'^+\overleftrightarrow{\partial}^{\mu}H_2'^{--}$	$-\frac{ig}{\sqrt{2}}$	$Z_{1\mu}H_1'^+\overleftrightarrow{\partial}^{\mu}H_1'^-$	$-\frac{ig(1+2s_W^2)}{2c_W}$
$Z_{2\mu}H_1'^+\overleftrightarrow{\partial}^{\mu}H_1'^-$	$-\frac{ig(1-10s_W^2)}{2\sqrt{3}c_W\sqrt{1-4s_W^2}}$	$A_\mu H_2'^+\overleftrightarrow{\partial}^{\mu}H_2'^-$	$2igs_W$
$W_\mu^-H_2'^{++}\overleftrightarrow{\partial}^{\mu}H_1'^-$	$-\frac{ig}{\sqrt{2}}$	$Z_{1\mu}H_2'^{++}\overleftrightarrow{\partial}^{\mu}H_2'^{--}$	$\frac{ig(1-4s_W^2)}{2c_W}$
$Z_{2\mu}H_2'^{++}\overleftrightarrow{\partial}^{\mu}H_2'^{--}$	$-\frac{ig(1-10s_W^2)}{2\sqrt{3}c_W\sqrt{1-4s_W^2}}$		

The interactions of inert scalars with normal Higgs bosons in this model are given in Table IV, while the gauge-inert field interactions are listed in Table V and Table VI.

APPENDIX C: FEYNMAN DIAGRAMS

For the reader's convenience, we will list the Feynman diagrams for dark-matter (co)annihilation processes. The annihilation channels of H_1' are given in Fig. 9.

Since the candidate H_3' is the Standard Model singlet, it does not interact with the Standard Model gauge bosons as H_1' does. Excluding these elements, the remaining annihilation channels of H_1' are almost similar to H_3' by the replacement $H_1' \to H_3'$ and $A_1' \to A_3'$. Figure 10 lists only the channels that are different from those of H_1'. We see that there is only one possible diagram for each $H_3'H_3' \to Z_1Z_1; Z_1Z_2; W^+W^-$ via the Higgs portals (less than the number of diagrams corresponding to H_1' annihilation, as noted) while there are additionally possibilities of $H_3'H_3' \to Y^{++}Y^{--}$.

TABLE VI. Quartic interactions of inert scalars with gauge bosons in the χ' model.

Vertex	Coupling	Vertex	Coupling
$H_3'H_3'Y^{++}Y^{--}$	$\frac{g^2}{4}$	$H_3'H_3'X^+X^-$	$\frac{g^2}{4}$
$H_3'H_3'Z_2Z_2$	$\frac{g^2c_W^2}{6(1-4s_W^2)}$	$A_3'A_3'Y^{++}Y^{--}$	$\frac{g^2}{4}$
$A_3'A_3'X^+X^-$	$\frac{g^2}{4}$	$A_3'A_3'Z_2Z_2$	$\frac{g^2c_W^2}{6(1-4s_W^2)}$
$H_3'H_1'^+AX^-$	$-\frac{g^2s_W}{2}$	$H_3'H_1'^+W^+Y^{--}$	$\frac{g^2}{2\sqrt{2}}$
$H_3'H_1'^+Z_1X^-$	$\frac{g^2(1+2s_W^2)}{4c_W}$	$H_3'H_1'^+Z_2X^-$	$-\frac{g^2(1+8s_W^2)}{4\sqrt{3}c_W\sqrt{1-4s_W^2}}$
$H_3'H_2'^{++}W^-X^-$	$\frac{g^2}{2\sqrt{2}}$	$H_3'H_2'^{++}AY^{--}$	$-g^2s_W$
$H_3'H_2'^{++}Z_1Y^{--}$	$-\frac{g^2(1-4s_W^2)}{4c_W}$	$H_3'H_2'^{++}Z_2Y^{--}$	$-\frac{g^2(1+8s_W^2)}{4\sqrt{3}c_W\sqrt{1-4s_W^2}}$
$A_3'H_1'^+AX^-$	$-\frac{ig^2s_W}{2}$	$A_3'H_1'^+W^+Y^{--}$	$\frac{ig^2}{2\sqrt{2}}$
$A_3'H_1'^+Z_1X^-$	$\frac{ig^2(1+2s_W^2)}{4c_W}$	$A_3'H_1'^+Z_2X^-$	$-\frac{ig^2(1+8s_W^2)}{4\sqrt{3}c_W\sqrt{1-4s_W^2}}$
$A_3'H_2'^{++}W^-X^-$	$\frac{ig^2}{2\sqrt{2}}$	$A_3'H_2'^{++}AY^{--}$	$-ig^2s_W$
$A_3'H_2'^{++}Z_1Y^{--}$	$-\frac{ig^2(1-4s_W^2)}{4c_W}$	$A_3'H_2'^{++}Z_2Y^{--}$	$-\frac{g^2(1+8s_W^2)}{4\sqrt{3}c_W\sqrt{1-4s_W^2}}$
$H_1'^+H_2'^{--}AW^+$	$-\frac{3g^2s_W}{\sqrt{2}}$	$H_1'^+H_2'^{--}X^-Y^{++}$	$\frac{g^2}{2}$
$H_1'^+H_2'^{--}Z_1W^+$	$\frac{3g^2s_Wt_W}{\sqrt{2}}$	$H_1'^+H_2'^{--}Z_2W^+$	$\frac{g^2(1-10s_W^2)}{\sqrt{6}c_W\sqrt{1-4s_W^2}}$
$H_1'^+H_1'^-AA$	$g^2s_W^2$	$H_1'^+H_1'^-AZ_1$	$-g^2t_W(1+2s_W^2)$
$H_1'^+H_1'^-AZ_2$	$-\frac{g^2t_W(1-10s_W^2)}{\sqrt{3}\sqrt{1-4s_W^2}}$	$H_1'^+H_1'^-W^+W^-$	$\frac{g^2}{2}$
$H_1'^+H_1'^-X^+X^-$	$\frac{g^2}{2}$	$H_1'^+H_1'^-Z_1Z_1$	$\frac{g^2(1+2s_W^2)^2}{4c_W^2}$
$H_1'^+H_1'^-Z_1Z_2$	$\frac{g^2(1+2s_W^2)(1-10s_W^2)}{2\sqrt{3}c_W^2\sqrt{1-4s_W^2}}$	$H_1'^+H_1'^-Z_2Z_2$	$\frac{g^2(1-10s_W^2)^2}{12c_W^2(1-4s_W^2)}$
$H_2'^{++}H_2'^{--}AA$	$4g^2s_W^2$	$H_2'^{++}H_2'^{--}AZ_1$	$2g^2t_W(1-4s_W^2)$
$H_2'^{++}H_2'^{--}AZ_2$	$-\frac{2g^2t_W(1-10s_W^2)}{\sqrt{3}\sqrt{1-4s_W^2}}$	$H_2'^{++}H_2'^{--}W^+W^-$	$\frac{g^2}{2}$
$H_2'^{++}H_2'^{--}Y^{++}Y^{--}$	$\frac{g^2}{2}$	$H_2'^{++}H_2'^{--}Z_1Z_1$	$\frac{g^2(1-4s_W^2)^2}{4c_W^2}$
$H_2'^{++}H_2'^{--}Z_1Z_2$	$-\frac{g^2(1-4s_W^2)(1-10s_W^2)}{2\sqrt{3}c_W^2\sqrt{1-4s_W^2}}$	$H_2'^{++}H_2'^{--}Z_2Z_2$	$\frac{g^2(1-10s_W^2)^2}{12c_W^2(1-4s_W^2)}$

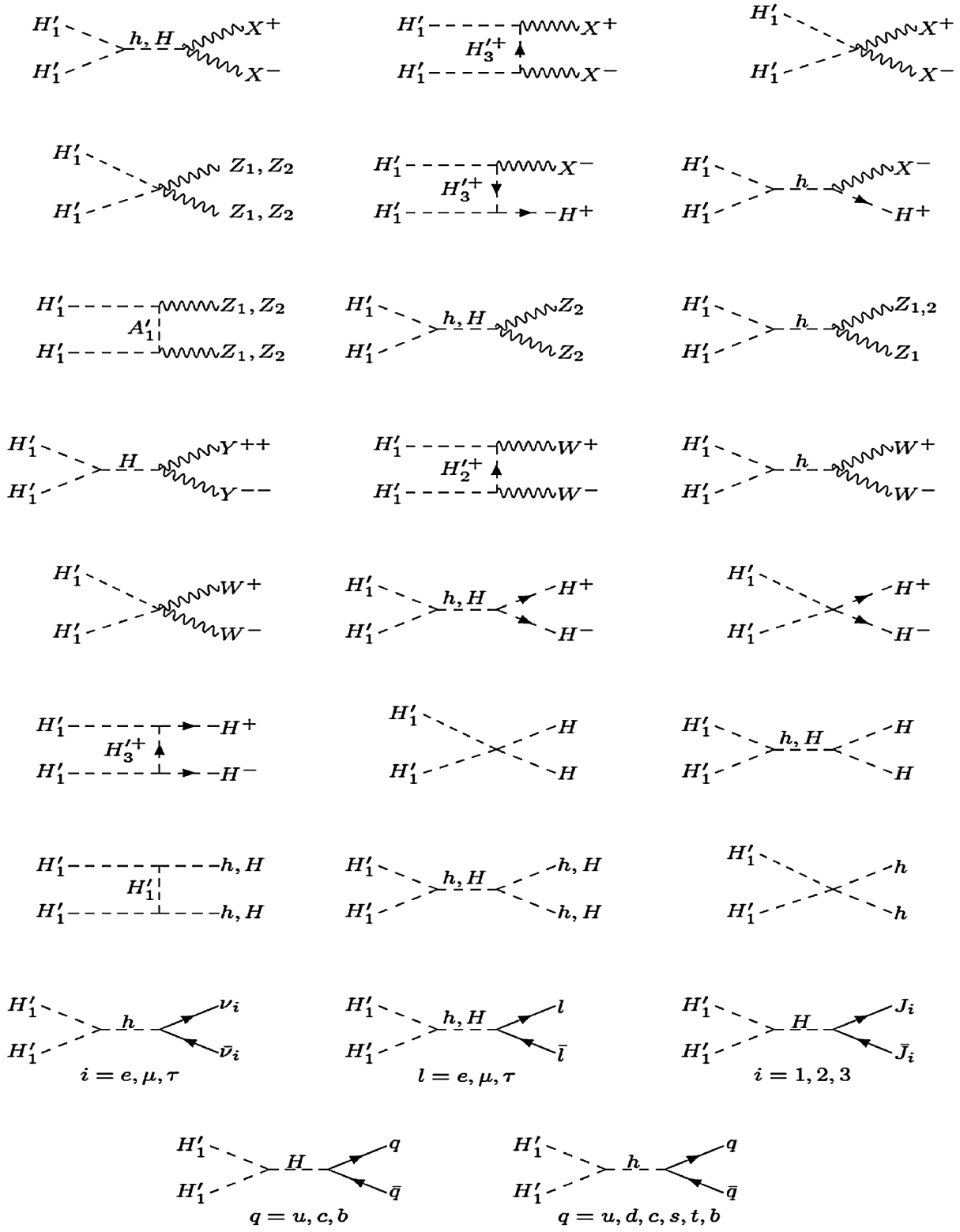

FIG. 9. Diagrams contributing to the annihilation of H_1' dark matter.

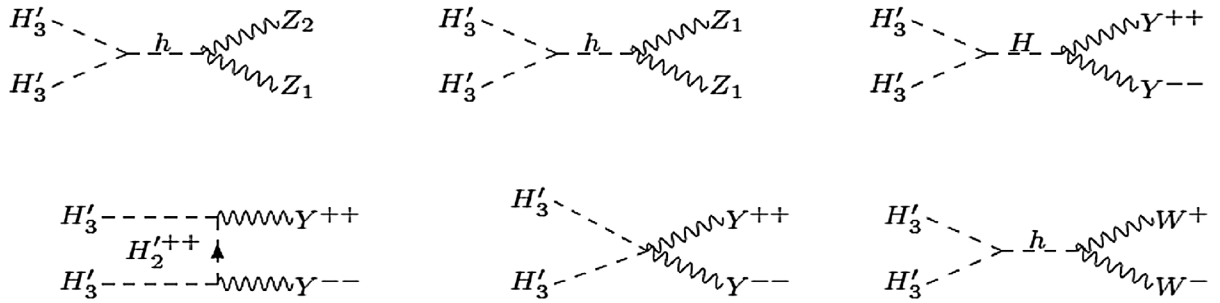

FIG. 10. Diagrams contributing to the annihilation of H_3' dark matter. We only list the channels that are different from those that are due to the annihilation of H_1'.

[1] D. N. Spergel *et al.* (WMAP Collaboration), Astrophys. J. Suppl. Ser. **170**, 377 (2007); P. A. R. Ade *et al.* (Planck Collaboration), Astron. Astrophys. **571**, A1 (2014).

[2] G. Jungman, M. Kamionkowski, and K. Griest, Phys. Rep. **267**, 195 (1996); G. Bertone, D. Hooper, and J. Silk, Phys. Rep. **405**, 279 (2005); H. Murayama, arXiv:0704.2276; S. Dodelson and L. M. Widrow, Phys. Rev. Lett. **72**, 17 (1994); C. Boehm and P. Fayet, Nucl. Phys. **B683**, 219 (2004); D. Fargion and M. Yu. Khlopov, Gravitation Cosmol. **19**, 219 (2013); S. B. Gudnason, C. Kouvaris, and F. Sannino, Phys. Rev. D **74**, 095008 (2006); S. B. Gudnason, C. Kouvaris, and F. Sannino, Phys. Rev. D **73**, 115003 (2006); D. Fargion, M. Yu. Khlopov, and C. A. Stephan, Classical Quantum Gravity **23**, 7305 (2006); M. Yu. Khlopov, JETP Lett. **83**, 1 (2006) [Pisma Zh. Eksp. Teor. Fiz. **83**, 3 (2006)].C. G. Boehmer and T. Harko, J. Cosmol. Astropart. Phys. 06 (2007) 025; C. Kouvaris, Phys. Rev. D **76**, 015011 (2007); M. Yu. Khlopov and C. Kouvaris, Phys. Rev. D **77**, 065002 (2008); K. Hamaguchi, S. Shirai, and T. T. Yanagida, Phys. Lett. B **654**, 110 (2007); G. Belanger, A. Pukhov, and G. Servant, J. Cosmol. Astropart. Phys. 01 (2008) 009; H. S. Cheng, J. L. Feng, and K. T. Matchev, Phys. Rev. Lett. **89**, 211301 (2002); G. Servant and T. M. P. Tait, New J. Phys. **4**, 99 (2002); Nucl. Phys. **B650**, 391 (2003); F. Fucito, A. Lionetto, and M. Prisco, J. Cosmol. Astropart. Phys. 06 (2006) 002; K. Hsieh, R. N. Mohapatra, and S. Nasri, Phys. Rev. D **74**, 066004 (2006); J. High Energy Phys. 12 (2006) 067; M. Regis, M. Serone, and P. Ullio, J. High Energy Phys. 03 (2007) 084; D. Hooper and S. Profumo, Phys. Rep. **453**, 29 (2007); S. Matsumoto, J. Sato, M. Senami, and M. Yamanaka, Phys. Rev. D **76**, 043528 (2007); B. A. Dobrescu, D. Hooper, K. Kong, and R. Mahbubani, J. Cosmol. Astropart. Phys. 10 (2007) 012; A. Martin, arXiv:hep-ph/0602206; A. Birkedal, A. Noble, M. Perelstein, and A. Spray, Phys. Rev. D **74**, 035002 (2006); C. S. Chen, K. Cheung, and T. C. Yuan, Phys. Lett. B **644**, 158 (2007); M. Perelstein and A. Spray, Phys. Rev. D **75**, 083519 (2007); D. Hooper and G. Zaharijas, Phys. Rev. D **75**, 035010 (2007).

[3] F. Pisano and V. Pleitez, Phys. Rev. D **46**, 410 (1992); P. H. Frampton, Phys. Rev. Lett. **69**, 2889 (1992); R. Foot, O. F. Hernandez, F. Pisano, and V. Pleitez, Phys. Rev. D **47**, 4158 (1993).

[4] M. Singer, J. W. F. Valle, and J. Schechter, Phys. Rev. D **22**, 738 (1980); R. Foot, H. N. Long, and T. A. Tran, Phys. Rev. D **50**, R34 (1994); J. C. Montero, F. Pisano, and V. Pleitez, Phys. Rev. D **47**, 2918 (1993); H. N. Long, Phys. Rev. D **54**, 4691 (1996); **53**, 437 (1996).

[5] D. Ng, Phys. Rev. D **49**, 4805 (1994); D. G. Dumm, F. Pisano, and V. Pleitez, Mod. Phys. Lett. A **09**, 1609 (1994); H. N. Long and V. T. Van, J. Phys. G **25**, 2319 (1999).

[6] F. Pisano, Mod. Phys. Lett A **11**, 2639 (1996); A. Doff and F. Pisano, Mod. Phys. Lett. A **14**, 1133 (1999); C. A. de S. Pires and O. P. Ravinez, Phys. Rev. D **58**, 035008 (1998); C. A. de S. Pires, Phys. Rev. D **60**, 075013 (1999); P. V. Dong and H. N. Long, Int. J. Mod. Phys. A **21**, 6677 (2006).

[7] M. B. Tully and G. C. Joshi, Phys. Rev. D **64**, 011301 (2001); A. G. Dias, C. A. de S. Pires, and P. S. Rodrigues da Silva, Phys. Lett. B **628**, 85 (2005); D. Chang and H. N. Long, Phys. Rev. D **73**, 053006 (2006); P. V. Dong, H. N. Long, and D. V. Soa, Phys. Rev. D **75**, 073006 (2007); **77**, 057302 (2008); P. V. Dong, L. T. Hue, H. N. Long, and D. V. Soa, Phys. Rev. D **81**, 053004 (2010); P. V. Dong, H. N. Long, D. V. Soa, and V. V. Vien, Eur. Phys. J. C **71**, 1544 (2011); P. V. Dong, H. N. Long, C. H. Nam, and V. V. Vien, Phys. Rev. D **85**, 053001 (2012); S. M. Boucenna, S. Morisi, and J. W. F. Valle, Phys. Rev. D **90**, 013005 (2014).

[8] D. Fregolente and M. D. Tonasse, Phys. Lett. B **555**, 7 (2003); H. N. Long and N. Q. Lan, Europhys. Lett. **64**, 571 (2003); S. Filippi, W. A. Ponce, and L. A. Sanches, Europhys. Lett. **73**, 142 (2006); C. A. de S. Pires and P. S. Rodrigues da Silva, J. Cosmol. Astropart. Phys. 12 (2007) 012; J. K. Mizukoshi, C. A. de S. Pires, F. S. Queiroz, and P. S. Rodrigues da Silva, Phys. Rev. D **83**, 065024 (2011); J. D. Ruiz-Alvarez, C. A. de S. Pires, F. S. Queiroz, D. Restrepo, and P. S. Rodrigues da Silva, Phys. Rev. D **86**, 075011 (2012); S. Profumo and F. S. Queiroz, Eur. Phys. J. C **74**, 2960 (2014); C. Kelso, C. A. de S. Pires, S. Profumo, F. S. Queiroz, and P. S. Rodrigues da Silva, Eur. Phys. J. C **74**, 2797 (2014); P. S. Rodrigues da Silva, arXiv:1412.8633; F. S. Queiroz, AIP Conf. Proc. **1604**, 83 (2014); D. Cogollo, Alma X. Gonzalez-Morales, F. S. Queiro, and P. R. Teles, J. Cosmol. Astropart.

Phys. 11 (2014) 002; C. Kelso, H. N. Long, R. Martinez, and F. S. Queiroz, Phys. Rev. D **90**, 113011 (2014).
[9] P. V. Dong, T. D. Tham, and H. T. Hung, Phys. Rev. D **87**, 115003 (2013); P. V. Dong, D. T. Huong, F. S. Queiroz, and N. T. Thuy, Phys. Rev. D **90**, 075021 (2014); D. T. Huong, P. V. Dong, C. S. Kim, and N. T. Thuy, Phys. Rev. D **91**, 055023 (2015).
[10] P. V. Dong, T. Phong Nguyen, and D. V. Soa, Phys. Rev. D **88**, 095014 (2013).
[11] P. V. Dong, N. T. K. Ngan, and D. V. Soa, Phys. Rev. D **90**, 075019 (2014).
[12] N. G. Deshpande and E. Ma, Phys. Rev. D **18**, 2574 (1978); L. L. Honorez, E. Nezri, J. F. Oliver, and M. H. G. Tytgat, J. Cosmol. Astropart. Phys. 02 (2007) 028; M. Cirelli, N. Fornengo, and A. Strumia, Nucl. Phys. **B753**, 178 (2006); T. Hambye, F. S. Ling, L. Lopez Honorez, and J. Rocher, J. High Energy Phys. 07 (2009) 090.
[13] J. G. Ferreira, Jr., P. R. D. Pinheiro, C. A. de S. Pires, and P. S. Rodrigues da Silva, Phys. Rev. D **84**, 095019 (2011).
[14] P. V. Dong and D. T. Si, Phys. Rev. D **90**, 117703 (2014).
[15] P. V. Dong and H. N. Long, Eur. Phys. J. C **42**, 325 (2005).
[16] R. Barbieri, L. J. Hall, and V. S. Rychkov, Phys. Rev. D **74**, 015007 (2006).
[17] V. Silveira and A. Zee, Phys. Lett. **161B**, 136 (1985); K.-M. Cheung, Y.-L. S. Tsai, P.-Y. Tseng, T.-C. Yuan, and A. Zee, J. Cosmol. Astropart. Phys. 10 (2012) 042; J. M. Cline, P. Scott, K. Kainulainen, and C. Weniger, Phys. Rev. D **88**, 055025 (2013).
[18] G. Belanger, F. Boudjema, P. Brun, A. Pukhov, S. Rosier-Lees, P. Salati, and A. Semenov, Comput. Phys. Commun. **182**, 842 (2011).
[19] G. Belanger, F. Boudjema, A. Pukhov, and A. Semenov, Comput. Phys. Commun. **180**, 747 (2009).
[20] A. Pukhov, arXiv:hep-ph/0412191.
[21] K. Griest and D. Seckel, Phys. Rev. D **43**, 3191 (1991).
[22] M. M. Pavan, I. I. Strakovsky, R. L. Workman, and R. A. Arndt, PiN Newslett. **16**, 110 (2002). arXiv:hep-ph/0111066
[23] E. Komatsu *et al.*, Astrophys. J. Suppl. Ser. **192**, 18 (2011).
[24] M. Cirelli, N. Fornengo, and A. Strumia, Nucl. Phys. **B753**, 178 (2006).
[25] A. G. Dias, R. Martinez, and V. Pleitez, Eur. Phys. J. C **39**, 101 (2005).
[26] J. Ellis, A. Ferstl, and K. A. Olive, Phys. Lett. B **481**, 304 (2000).
[27] J. Beringer *et al.* (Particle Data Group), Phys. Rev. D **86**, 010001 (2012).